出國報告(出國類別：進修)

美國西雅圖華盛頓大學醫學院
肝膽及腸胃道病理進修

服務機關：國防醫學院病寄所
姓名職稱：彭奕仁 中校教師
派赴國家/地區：美國/西雅圖
出國期間：108 年 8 月 30 日 109 年至 7 月 29 日
報告日期：109 年 8 月 8 日

摘要

至美國西雅圖華盛頓大學醫學院附設醫院進修一年，與 Matthew Yeh 教授學習肝膽及腸胃道病理學，診斷與相關研究。後半年因遇到全球新冠病毒疫情，學習方式有所調整。心得與建議如下：(1)完善病理次專科訓練制度：在精準醫療的年代，建議三總病理部每位主治醫師著重發展一至二個次專科領域，參加院外會議與各次專科分委會，從美國經驗來看這是一個不可擋的趨勢；(2)健全會診制度：以病人安全為優先，善用跨院會診制度。(3)學習台灣少見個案：因人種及地區性，學習西方不同病理診斷，隨著台灣走向國際化，類似的個案應該會增加；(4)優化病理報告處理流程的專業分工與授權。(5) 人性化的病理報告系統：需要與資訊人員合作協商；(6)資料庫的應用：整合病理與臨床資訊，用於資料分析與病理研究；(7)維持病理與臨床的溝通討論；(8) 與教授學習批評性評論（Critical review）；(9) 參與研究主題。

目次   頁數

目的

因應三軍總醫院病理部科別發展需要，至美國西雅圖華盛頓大學醫學院附設醫院，與 Matthew Yeh 教授學習肝膽及腸胃道病理學，診斷與相關研究。

過程

國防部提供至美國短期進修一年，後半年因遇到全球新冠病毒疫情，學習方式有所調整。原訂最後三個月與腎臟病理 Kelly Smith 教授學習，因新冠病毒疫情而取消，也因疫情嚴峻決定提早一個月返台。

學習肝臟病理診斷與常規參與會議：

週中常規參與指導教授一同閱片及診斷，在多人頭顯微鏡教學室，以實際案例學習。

每週二、三上午固定臨床病理肝臟腫瘤會議，每週三下午有肝臟移植病理討論會議。與臨床醫生共同討論病情，確認診斷與後續治療。

參與教授研究：

除臨床診斷之外，也參與肝膽及腸胃道病理研究：

9 月至 10 月：主題為非酒精性脂肪肝炎，整理教授手上美國非酒精性脂肪肝炎病理資料庫，按最新分類，將病理變化與臨床資料配對，以生物統計的方法找尋預後指標。

11 月至 12 月：以 2018 年新版 WHO 肝臟病理共識，重新分類診斷過去 10 年在華盛頓大學附設醫院合併型肝細胞癌與肝內膽管癌(combined hepatocellular carcinoma and cholangiocarcinoma)，比較兩者的差異性與預後。

1 月至 2 月：主題為 hepatic angiomyolipoma，以免疫組織化學染色評估腫瘤的成因與病人的預後關聯，尋找新的至病路徑，包含 p53 及 pS6/mTOR signaling。

3 月之後：美國冠狀病毒疫情升溫，在我居住的華盛頓州 King county 也有疫情傳出。美國人沒有戴口罩的習慣，一般認為只有生病的人才要戴口罩，再者美國槍枝合法，遮掩顏面會使人產生將行不法行動的誤會，而不戴口罩這給無症狀患者一個傳播的機會。期間疫情較為緊張，口罩、酒精、衛生紙賣到缺貨。我也囤積了一些生活用品(米、罐頭、衛生紙等)，以備不時之需。當中還有警察執法過當造成種族事件，引起全美國示威抗議，部分城市發生暴力事件。指導教授指示三月中起先留在家中，暫不到醫院，改以在家學習與線上討論。原定最後三個月至腎臟部門學習因而取消，甚可惜。教授借我研究玻片與一台顯微鏡放置家中，可以在家學習與線上討論。論文已開撰寫，但一部分實驗還未完成，回國後仍與教授聯絡進行中。

心得與參與研究：

1. 完善的病理次專科訓練制度

美國解剖病理有完整的次專科訓練及認證，包含肝膽腸胃次專科，神經病理次專科、皮膚病理次專科等。各次專科專注在自己的領域，台灣解剖病理近年也往次專科的方向發展，成立各次專科分委會，但還沒有證照制度。國內因病理專科人數有限，一般醫院很難做到次分科，只有在少數醫學中心採行。在精準醫療的年代，建議三總病理部每位主治醫師著重發展一至二個次專科領域，參加院外會議與各次專科分委會，從美國經驗來看這是一個不可擋的趨勢。

2. 健全的會診制度與台灣少見個案

美國西雅圖華盛頓大學醫學院附設醫院為華盛頓州的醫學中心，周圍地區醫院病理科有疑難個案都會會診至該中心，看到許多在台灣少見的個案，如 inflammatory bowel disease, autoimmune hepatitis, Celiac disease 這裡很常見，但在台灣一年只有幾個個案。當然也是與人種及地區性流行病學有關，隨著台灣邁向國際醫療與人種多樣性，再看到類似個案會有把握抓住診斷的依據。

3. 病理報告處理流程的分工與授權

從檢體外觀拍照記錄、錄音紀錄、取樣、包埋、切片、染色、謄打報告，都有每個步驟

都有專人專業分工，在病理報告中都有詳細記錄，並署名以示負責，這在英文為母語的國家是具有優勢的。這幾年台灣病理學會也有往該方向發展，如開辦課程訓練醫檢師處理檢體並完善紀錄。我出國前三總病理部也開始訓練醫檢師更多參與病理作業，英文能力是一個問題，若之後還有招聘新人，建議要將英文能力納入考核，設定托福、多益或全民英檢的最低門檻，以利後續訓練。

4. 人性化的病理報告系統

華大病理部的病理報告系統整合最新版ＴＮＭ，輸入相關資料病理分期就會自動跳出，當然這需要強大的資訊團隊支援，減少人為錯誤。Matthew Yeh 教授注重與臨床的溝通，尤其是在非腫瘤性的切片，他會列出可能的鑑別診斷，並電話與臨床主治醫師溝通，這點是值得學習的。

5. 完善資料系統便於資料分析與病理研究

資訊系統包含門診與住院資料、影像、實驗室分析與資料搜尋，當有研究想法時，很容易從資料庫找個相關個案。有分配專門的研究人力，除診斷外免疫組織化學染色，分子檢測都可以提出申請，這一部分三總也在努力追趕中，

6. 病理與臨床的溝通討論

每週固定有肝膽癌症治療討論會、肝臟移植病理討論會、病理與影像討論會，注重與臨床團隊的討論，包含診斷（腸胃內科、放射科）、治療（腸胃內科、一般外科、腫瘤科、放射治療科）、移植團隊。這一部分三總也有類似的會議。

7. 學習批評性評論（Critical review）

Matthew Yeh 教授是知名的肝臟病理專家，常有優良肝膽領域期刊找他審稿。他對我的訓練包含批評性評論寫作，我做完批評性評論後他再整合自己的意見，在回覆雜誌社時也會將他的意見回饋給我，給我不同的視角，在受訓期間共有約有三十篇，在論文寫作與

回覆上我也有所精進，我也整理出自己的回覆套路，這對與我之後文章投稿也有幫助。

8. 參與研究主題如下：

A. **評估胰臟線管細胞癌**(pancreas ductal adenocarcinoma, PDCA)組織矩陣與染色結果分析。
胰臟線管細胞癌為預後及差的癌症，者要原因是症狀不明顯，往往發現時已是末期，
本研究發現一轉錄因子(transcriptional factor)蛋白質與 PDCA 的侵襲性與遇後有關，表
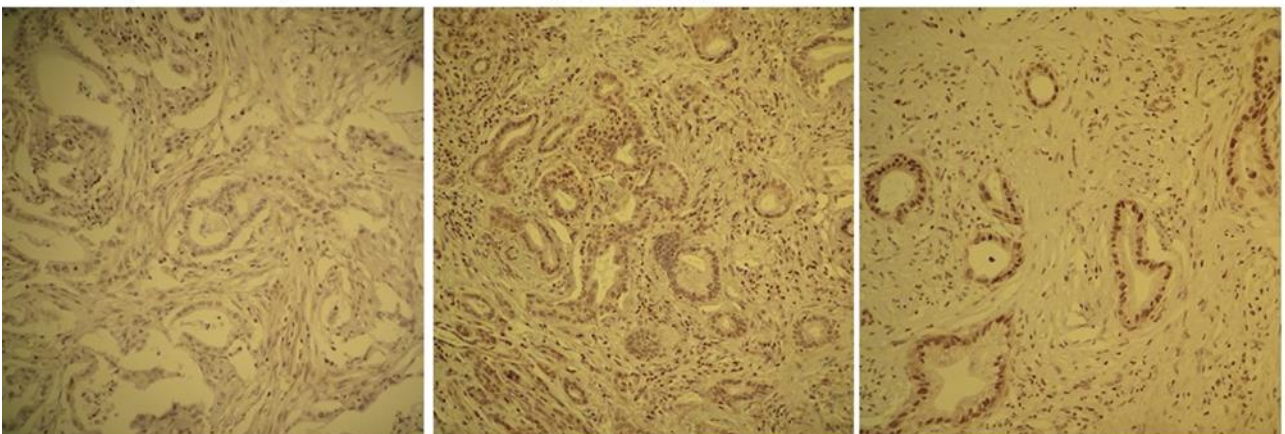現於細胞核。我接續前人的研究，做型態與免疫組織化學染色的分析，並與臨床資料
對比，類似研究我之前在台灣有做過，因此執行起來得心應手。

Four TMA slides with number
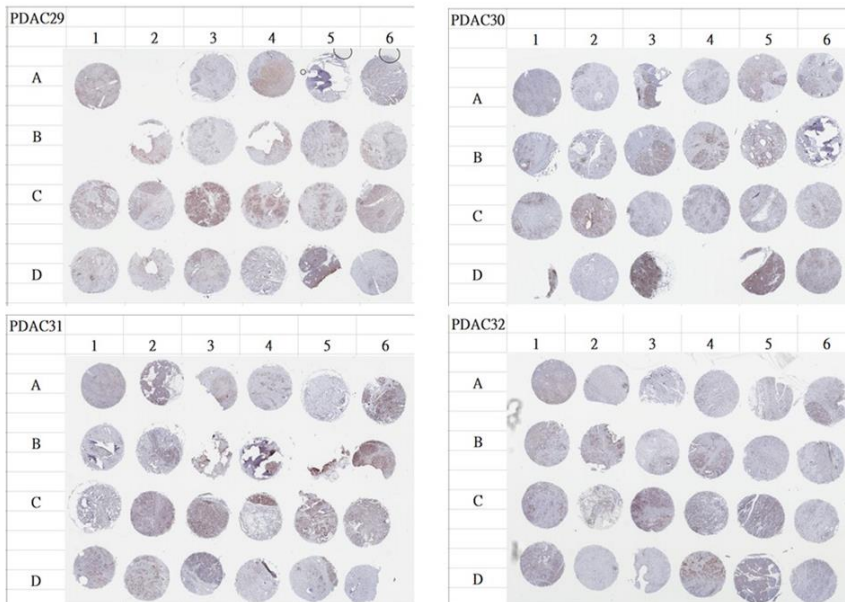
Score 0+
(PDAC29 D4)

Score 1+
(PDAC32 C3)

Score 2+
(PDAC29 C5)

B. 小鼠非酒精性脂肪肝評估與分析

這是 Matthew Yeh 教授與基礎學科的合作計畫，這裡看了很多非酒精性脂肪肝個案，我按此診斷標準，針對 50 隻小鼠疾病組與治療組肝臟切片做評估，這項參與讓我對非酒精性脂肪肝評估標準更加熟悉。

C. 肝臟骨隨外造血研究

骨隨外造血並在肝臟以腫瘤形式呈現並不常見。在 Matthew Yeh 教授指導下，分析 2000 至 2015 間，華盛頓大學醫學院所收集到的 9 個個案，並與過去個案做系統性分析。這是**延續完成之前的研究，現論文已完成，投稿中，首頁及摘要如下：**

Extramedullary Hematopoiesis Presenting as Focal Lesions in the Liver: A Pathological and Radiological Study

Marife J. Bonifacio, MD[1], Gregory Cheeney, MD[1], **Yi-Jen Peng**, MD, PhD[1,2], Carlos Cuevas, MD[3], Matthew M. Yeh, MD, PhD[1,4]

[1]University of Washington, Department of Pathology, Seattle, WA, United States.

[2]Tri-Service General Hospital, National Defense Medical Center, Department of Pathology, Taipei, Taiwan.

[3]University of Washington, Department of Radiology, Seattle, WA, United States.

[4]University of Washington, Department of Medicine, Seattle, WA, United States.

Corresponding author:
Matthew M Yeh, MD, PhD
Department of Pathology
University of Washington School of Medicine
1959 NE Pacific Street, NE140D
Box 356100
Seattle, WA 98195
Telephone:　206-598-0008

Fax: 206-598-4928

Email: myeh@uw.edu

Abstract

Background: Intrahepatic extramedullary hematopoiesis (EMH) presenting as focal lesions is a rare and uncommon entity. It is not frequently considered when seen on imaging studies but is only incidentally found on pathologic examination. The aim of this study is to examine the histomorphologic and imaging characteristics of these focal liver lesions and to assess the clinical setting of its occurrence. Here we present a series of 9 patients with confirmed EMH of the liver seen as focal lesions on cross-sectional imaging. **Methods:** We reviewed the electronic database from the Department of Pathology at the University of Washington Medical Center between the year 2000 to 2015 and identified 9 patients with EMH presenting with focal lesion(s) on radiologic imaging. Hematoxylin & Eosin-stained sections were reviewed retrospectively along with the cross-sectional imaging. These were cross referenced with available clinical data. **Results:** The cases included 4 men and 5 women, ranging from 18-71 years old (mean 54.7 years; median 60 years). The size of the lesions ranged from 0.6 cm to 2.2 cm in single widest dimension. All cases (n=9) showed trilineage hematopoiesis consisting predominantly of immature erythroid precursors and occasional myeloid cell clusters and megakaryocytes, all occupying the sinusoids. About half (5/9) of the patients had hematological disorders, with the remaining cases of patients from screening cirrhosis protocols (2/9) and metastatic disease work up (1/9). On cross-sectional imaging, 7 were multifocal and 2 were unifocal. Imaging findings on contrast-enhanced CT (n=7) showed low attenuation on venous phase on 5 cases and hyperattenuation on 2 cases. MR (n=2) showed enhancement in the arterial phase and wash out on delayed phase. All multiphase CT or MR imaging (n=4) showed arterial phase enhancement. Most cases (n=5) of retrospectively identified hepatic EMH were classified as indeterminate for definite diagnosis(n=6), and the rest as focal biliary dilation (n=1) and part of regenerative nodules (n=2).

Conclusion: Focal intrahepatic EMH are uncommon and can be diagnosed combining pathologic, radiologic and clinical findings. It should be considered in the differential diagnosis of lesions with hepatic sinusoidal infiltrates, particularly in the presence of hematologic malignancy or hemoglobinopathies. A high degree of suspicion should be maintained clinically as the imaging findings are usually nonspecific.

D. 肝臟血管肌肉脂肪瘤（hepatic angiomyolipoma, hepatic AML）的致病機轉。

Hepatic AML 為肝臟少見的腫瘤，該研究由美國與日本蒐集了 15 個個案，分析形態學，免疫組織化學染色與臨床預後。初步推斷與 renal AML 類似，突變與 TSC/mTOR 路徑有關，另 epithelioid variant 與 p53 mutation 有關。其中數個免疫組織化學染色因新冠病毒疫情而延後，在回台之前未能完成，後續與 Matthew Yeh 教授在做聯絡。

E. **在美期間文章發表**。整理之前國內研究資料，與指導教授討論並投稿，於 109 年六月與七月各刊登一篇學術論文，本人皆為第一作者。

(1) Decoy Receptor 3 Promotes Preosteoclast Cell Death via Reactive Oxygen Species-Induced Fas Ligand Expression and the IL-1 α/IL-1 Receptor Antagonist Pathway.

Peng YJ, Peng CT, Lin YH, Lin GJ, Huang SH, Chen SJ, Sytwu HK, Cheng CP.

Mediators Inflamm. 2020 Jun 10;2020:1237281. doi: 10.1155/2020/1237281.

(IF: 3.758, 63/158= 39.8%, IMMUNOLOGY)

(2) Astaxanthin attenuates joint inflammation induced by monosodium urate crystals.

Peng YJ, Lu JW, Liu FC, Lee CH, Lee HS, Ho YJ, Hsieh TH, Wu CC, Wang CC.

FASEB J. 2020 Jul 10. doi: 10.1096/fj.202000558RR. Online ahead of print.

(IF: 4.966, Ranking 9/93= 9.6%, BIOLOGY)

建議：

1. **發展次專科**：建議三總病理部每位主治醫師著重發展一至二個次專科領域，彼此能更專業的討論。鼓勵參加病理學會各次專科分委會與院外會議，累積人脈參與理監事選舉。

2. **健全會診制度**：以病人安全為中心，若科內討論無共識，藉由學會管道、各次專科分委會會診。現玻片數位化，會診國外專家學者較容易，當然要做分子檢驗仍需寄出實際的蠟塊檢體。

3. **發展可行性的精準醫療**。整合解剖病理、臨床病理、精準醫學暨基因體中心的資源，與臨床科別共同發展精準診斷與醫療。此發展初步可以臨床需要為導向，請臨床科別列出治療所需項目，經三單位與臨床需求單位討論分工與流程的建立。之前科內發展精準醫學，困難點在於沒錢(檢驗試劑費用)、沒人(操作技術員)，就現實面而言，賠錢的生意沒人做，找研究經費維持也不長久，臨床科別參與的重要性在於健保不給付項目，與病人解釋清楚後可請病人自費檢驗。

4. **病理報告處理流程的分工與授權(內部)**：參考國外經驗，醫檢師是一項高度專業的工作，

醫檢師的權責需區分清楚，在醫師的指導下，醫檢師執行檢體紀錄與取樣，這部分台灣病理學會已列入常規教育訓練，科內也在進行中，之後科內在招募人員需要將檢體處理操作與英文能力納入評量項目。

5. **完善資料系統便於資料分析與病理研究**：病理診斷需要整合病人臨床狀況、影像學、實驗室檢驗等，藉由資訊整合縮短蒐集資料時間；病理或臨床研究也需要有報告搜尋功能，作縱向整合。建立以需求為導向的病理資訊系統，連結臨床資料與搜尋功能。

Research Article

Decoy Receptor 3 Promotes Preosteoclast Cell Death via Reactive Oxygen Species-Induced Fas Ligand Expression and the IL-1α/IL-1 Receptor Antagonist Pathway

Yi-Jen Peng,[1] **Ching-Tsung Peng,**[2] **Yi-Hsuan Lin,**[3] **Gu-Jiun Lin,**[3] **Shing-Hwa Huang,**[3,4] **Shyi-Jou Chen** ,[5] **Huey-Kang Sytwu,**[5,6] **and Chia-Pi Cheng** [3]

[1]*Department of Pathology, Tri-Service General Hospital, National Defense Medical Center, Taipei, Taiwan*
[2]*Department of Clinical Pharmacy, Armed Forces Taoyuan General Hospital, Taoyuan, Taiwan*
[3]*Department and Graduate Institute of Biology and Anatomy, National Defense Medical Center, Taipei, Taiwan*
[4]*Department of General Surgery, Tri-Service General Hospital, National Defense Medical Center, Taipei, Taiwan*
[5]*Department and Graduate Institute of Microbiology and Immunology, National Defense Medical Center, Taipei, Taiwan*
[6]*National Health Research Institutes, Miaoli, Taiwan*

Correspondence should be addressed to Chia-Pi Cheng; ph870317@ndmctsgh.edu.tw

Purpose. Interleukin-1α (IL-1α) is a potent cytokine that plays a role in inflammatory arthritis and bone loss. Decoy receptor 3 (DCR3) is an immune modulator of monocytes and macrophages. The aim of this study was to investigate the mechanism of DCR3 in IL-1α-induced osteoclastogenesis. *Methods.* We treated murine macrophages with DCR3 during receptor activator of nuclear factor kappa B ligand- (RANKL-) plus IL-1α-induced osteoclastogenesis to monitor osteoclast formation by tartrate-resistant acid phosphatase (TRAP) staining. Osteoclast activity was assessed using a pit formation assay. The mechanisms of inhibition were studied by biochemical analyses, including RT-PCR, immunofluorescent staining, flow cytometry, an apoptosis assay, immunoblotting, and ELISA. *Results.* DCR3 suppresses IL-1α-induced osteoclastogenesis in both primary murine bone marrow-derived macrophages (BMM) and RAW264.7 cells as it inhibits bone resorption. DCR3 induces RANKL-treated osteoclast precursor cells to express IL-1α, secretory IL-1ra (sIL-1ra), intracellular IL-1ra (icIL-1ra), reactive oxygen species (ROS), and Fas ligand and to activate IL-1α-induced interleukin-1 receptor-associated kinase 4 (IRAK4). The suppression of DCR3 during RANKL- or IL-1α-induced osteoclastogenesis may be due to the abundant secretion of IL-1ra, accumulation of ROS, and expression of Fas ligand in apoptotic osteoclast precursor cells. *Conclusions.* We concluded that there is an inhibitory effect of DCR3 on osteoclastogenesis via ROS accumulation and ROS-induced Fas ligand, IL-1α, and IL-1ra expression. Our results suggested that the upregulation of DCR3 in preosteoclasts might be a therapeutic target in inflammatory IL-1α-induced bone resorption.

1. Introduction

Osteoclasts are differentiated from bone marrow-derived monocytes by stimulation of a critical factor, RANKL [1]. RANKL activation of its receptor RANK transduces downstream signals by recruiting TNF receptor-associated factors (TRAFs) [2]. This event triggers downstream signalling by stimulating its receptor RANK activating the nuclear factor κB (NF-κB) and mitogen-activated protein kinases (MAPKs) [3, 4]. The intracellular reactive oxidative stress (ROS) was also critically involved in RANKL/RANK signalling during osteoclastogenesis [5, 6]. IL-1 is known to be a potent cytokine in inflammatory regions, leading to bone erosion by activating osteoclasts [7, 8]. Overexpression of IL-1α in transgenic mice spontaneously induces polyarthritis [9, 10]. Furthermore, IL-1α has a synergistic effect in RANKL-stimulated osteoclastogenesis, which mediates TNF-α expression by directly stimulating the differentiation

of osteoclast precursors and inducing RANKL overexpression in stromal cells [11].

DCR3 is a soluble protein that belongs to the tumour necrosis factor receptor superfamily [12]. DCR3 interacts with its ligands, including TNFSF6 (FASLG), TNFSF14 (LIGHT), and TNFSF15 (TL1A) [13–15]. The function of DCR3 is to block or compete with ligand-receptor downstream signalling. Previous studies have shown that DCR3 plays multiple roles in the immune system. DCR3 prevents heart allograft rejection [16], promotes cancer cell growth by escaping immune surveillance [17, 18], and ameliorates many animal models of autoimmune diseases [19–22]. Researchers have also found that DCR3 can modulate macrophage and dendritic cell differentiation and maturation [23, 24]. Our previous studies found that DCR3 global expression attenuates the disease severity of collagen-induced arthritis in a mouse model and suppresses osteoclast differentiation in vitro [25, 26]. Moreover, DCR3 has been reported to activate IL-1ra expression in tumour-associated macrophages [27]. A previous study has reported that IL-1α and IL-1ra counterregulate each other in murine keratinocytes [28]. These findings give us a hint that DCR3 might be involved in IL-1α and IL-1ra regulation.

In the present study, we assessed the effects of DCR3 on RANKL- plus IL-1α-induced osteoclastogenesis in RAW264.7 cells and murine bone marrow-derived macrophage (BMM) cells. Moreover, we evaluated the possible mechanisms of DCR3 in osteolytic inflammation based on RANKL-induced osteoclastogenesis.

2. Materials and Methods

2.1. Cell Line and Reagents. The RAW264.7 cell line was obtained from the Food Industry Research and Development Institute (FIRDI) in Taiwan. Recombinant human DCR3 was purchased from R&D Systems Inc. (Minneapolis, MN, USA). Recombinant mouse RANKL, M-CSF, IL-1α, and anti-IL-1α were purchased from PeproTech (London, UK). Anti-IL-1ra was purchased from Abcam (Cambridge, UK). All other reagents were purchased from Sigma-Aldrich (St. Louis, MO, USA).

2.2. Cell Culture of Murine RAW264.7. The murine monocyte/macrophage cell line RAW264.7 was cultured with DMEM (Gibco, Dublin, Ireland) containing 10% heat-inactivated FBS, penicillin (100 U/ml), and streptomycin (100 μg/ml). All cells were grown in a humidified atmosphere containing 5% CO$_2$ at 37°C. To induce osteoclast differentiation, RAW264.7 cells were suspended in α-MEM containing 10% FBS, 100 U/ml penicillin, and 100 μg/ml streptomycin. Cells were seeded at a density of 1.5×10^4 cells/ml in each kind of plate (1 ml/well for a 24-well plate; 200 μl/well for a 96-well plate) and were stimulated with 50 ng/ml soluble RANKL alone or RANKL plus 50 ng/ml IL-1α concurrently treated with 10 μg/ml DCR3 or IgG control for 5 days. The medium was replaced on day 3. The safety dosage of 10 μg/ml DCR3 was used in RAW264.7 and BMM cells according to the previous studies by the cell viability assay [26, 29].

2.3. Cells Isolation and Osteoclast Differentiation. Bone marrow cells (BMMs) from normal DBA/1J mice tibia and femur bones were cultured overnight in α-MEM (Gibco BRL) supplemented with 10% heat-inactivated FBS, penicillin (100 U/ml), and streptomycin (100 μg/ml). Nonadherent cells were harvested and cultured in the presence of 30 ng/ml M-CSF, 50 ng/ml RANKL, and 50 ng/ml IL-1α as well as 10 μg/ml DCR3 or IgG for 5 days to generate osteoclasts. Cells were seeded at a density of 1×10^5 cells/ml in each kind of plate (1 ml/well for a 24-well plate; 200 μl/well for a 96-well plate). The medium was replaced on day 3.

2.4. Tartrate-Resistant Acid Phosphatase (TRAP) Staining. The cells were washed with PBS and fixed with 3.7% formaldehyde for 30 minutes. After washing with PBS, the cells were incubated at 37°C in a humid and light-protected incubator for 1 hour in the reaction mixture of a Leukocyte Acid Phosphatase Assay Kit (Cat. 387, Sigma-Aldrich) as directed by the manufacturer. The cells were washed three times with distilled water, and TRAP-positive multinucleated cells containing five or more nuclei were counted under a light microscope and photographed.

2.5. Pit Formation Assay. RAW264.7 cells were seeded onto 20 mm^2 dentine slices (Cat. 3988, Corning) in 24-well plates at a density of 10^5 cells per well. All the cultures were incubated in triplicate, and the cells were replenished every 3 days with fresh medium containing test articles. Then, the dentine slices were treated with 1 N NH$_4$OH with sonication for 5 minutes. Resorption pits on the dentine slices were visualized by staining with Mayer's Hematoxylin Solution (Sigma-Aldrich). The ratios of the resorbed area to the total area were measured in four optical fields on a slice using NIH Image software at 100-fold magnification.

2.6. RT-PCR and QPCR Analysis. Total RNA was isolated from the cultured cells using the TRIzol Reagent (Invitrogen, Carlsbad, CA, USA) and reverse transcribed using SuperScript III Reverse Transcriptase (Invitrogen). PCR was performed using mouse-specific primers as shown in sTable 1. Thermal cycling parameters were 95°C for 5 minutes, followed by 25~35 cycles for 30 seconds at 95°C, 30 seconds at 61°C, 1 minute at 72°C, and 10 minutes at 72°C for the final elongation. The number of cycles for each gene was determined to be in the range of linear amplification through an optimization experiment. PCR products were separated on 1.2% agarose gels, visualized by ethidium bromide staining, and analyzed densitometrically using a phosphorimager and Quantity One software. The optical densities for each gene were normalized to the corresponding values for glyceraldehyde-3-phosphate dehydrogenase (GAPDH). All markers of QPCR were analyzed by the LightCycler 480 II system (Roche, Mannheim, Germany). Quantitative thermal cycling parameters were 95°C for 15 minutes, followed by 40 cycles for 30 seconds at 95°C, 30 seconds at 61°C, and 1 minute at 72°C, as well as 10 minutes at 72°C for extension. The relative levels of each values were evaluated and normalized with GAPDH.

2.7. Immunoblotting Analysis. Whole cell extracts were prepared according to our previous study [30]. In brief, RAW264.7 cells treated with DCR3 or IgG control in the absence or presence of RANKL or IL-1α were harvested and suspended in RIPA lysis buffer containing protease and phosphatase inhibitors. Equivalent amounts of protein (20 μg/lane) were loaded into 10-15% SDS-PAGE for electrophoresis and transferred onto a polyvinylidene fluoride (PVDF) membrane. The membranes were blocked with 5% nonfat milk in PBST at room temperature for 1 hour twice to prevent nonspecific staining. Immunoblotting was performed using specific antibodies for IRAK4 (No. 4363), phospho-IRAK4 (No. 11927, Cell Signaling Technology, Danvers, MA, USA), IL-1α (No. 500-P51A stock concentration, 100 μg/ml, PeproTech, London, UK), IL-1ra (No. ab124962 stock concentration, 61 μg/ml, Abcam, Cambridge, UK), and GAPDH (No. 10494-1-AP stock concentration, 50 μg/150 μl, Proteintech Group, Rosemont, IL, USA). The membranes were incubated with primary antibodies at a diluted ratio of 1 : 1000 in room temperature for 1 hour. After washing three times in PBST for 10 mins, goat anti-rabbit secondary antibodies were added at diluted ratio of 1 : 2000 in room temperature for 1 hour. The immunoreactive bands were visualized with the enhanced chemiluminescent kit and analyzed by the VisionWorks LS UVP System. Each protein was measured by at least 3 times of repeated western blot analysis. The data were presented as the relative ratio of the target protein to the reference protein.

2.8. Immunofluorescent Staining. The distribution of IL-1α protein was assessed according to previously published protocols [31]. The cells were washed in PBS, fixed in 4% paraformaldehyde, permeabilized with 0.1% Triton X-100, incubated with 5% BSA, and then incubated with primary anti-IL-1α polyclonal antibody (1 : 50) at 4°C overnight. After overnight incubation, the cells were washed in PBS twice and incubated with secondary Alexa Fluor 488-conjugated donkey anti-rabbit IgG antibody for 2 hours (BioLegend, San Diego, CA, USA). After immunostaining, the cells were counterstained with the endoplasmic reticulum ER-ID® Red assay kit (Enzo Life Sciences, Farmingdale, NY, USA). Fluorescence was visualized using a Leica DMi8 fluorescence microscope at 40x magnification equipped with filters (A for Hoechst, GFP-EN for Alexa Fluor 488, and N21 for ER Texas Red) and analyzed by LAS EZ software.

2.9. Apoptosis Assays and Flow Cytometry. Cells were plated at a density of 10^5 cells per well in 24-well plates under the protocol of osteoclast differentiation. After 48 hours of incubation, the cells were stained with Annexin V-FITC and PI for evaluating cell apoptosis or stained with PE-conjugated anti-Fas ligand to evaluate death ligand expression by the BD FACSCalibur flow cytometry system equipped with fluorescence detectors and bandpass filters, 530 nm for FITC and 585 nm for PE/PI (BD Biosciences, NJ, USA). Cells were acquired and analyzed by using CellQuest Pro software.

2.10. ROS Assays. Cells were plated at a density of 10^5 cells per well in 24-well plates under the protocol of osteoclast differentiation. After 6 hours incubation, the CellROX Green Reagent (Invitrogen) was added to each well at a concentration of 5 μmol/l according to the manufacturer. After 30 minutes of incubation, cells were analyzed by flow cytometry (BD Biosciences, NJ, USA) with 530 nm bandpass filters for green fluorescence and CellQuest Pro software.

2.11. Enzyme-Linked Immunosorbent Assay. Whole cell lysate and culture medium of IL-1α and IL-1ra were measured using ELISAs according to the manufacturer (murine IL-1α from eBioscience and IL-1ra from R&D Systems). Briefly, equivalent amounts of total cell lysate (5 μg/well) or medium (100 μl/well) were loaded into the IL-1α and IL-1ra specific antibody-precoated well and incubated overnight at 4°C. After washing with 200 μl PBST 3 times, 100 μl of diluted detection antibody was added to each well and incubated at room temperature for 1 hour. After 3 washes, 100 μl Avidin-HRP was added to the wells and incubated at room temperature for 30 mins. After 5 washes, 100 μl of 1x TMB solution was added to the wells and incubated at room temperature for 15 mins. The intensity of the color was measured at an absorbance wavelength of 450 nm. The detection limits were 4 pg/ml for IL-1α and 13 pg/ml for IL-1ra.

2.12. Statistical Analysis. All the experiments were done for at least 3 independent repeats. Data were shown as the mean values ± SD and were analyzed using one-way ANOVA with the Newman-Keuls multiple comparisons on posttests. $P < 0.05$ was considered statistically significant.

3. Results

3.1. Effects of DCR3 on RANKL- Plus IL-1α-Induced Osteoclast Differentiation and Function. Investigating the suppressive effect of DCR3 in IL-1α-induced osteoclastogenesis was promising. RANKL-stimulated RAW264.7 cells were treated with DCR3 in the presence or absence of IL-1α. The results showed that the numbers of multinucleated osteoclasts decreased in the DCR3-treated group even when they underwent concurrent treatment with IL-1α (Figure 1(a)). In BMMs, the IL-1α-treated group was more dramatically increased in the RANKL-induced osteoclast formation as compared with RANKL treated alone. And, these suppressive effects of DCR3 were also reproduced by using primary murine BMMs (sFigure 1). To further examine the effects of DCR3 on the functions of osteoclastogenesis, we evaluated bone resorption activity by using a pit formation assay. The results showed that RANKL- plus IL-1α-evoked bone resorption was diminished in the presence of DCR3 (Figure 1(b)).

3.2. Effects of DCR3 on IL-1α and IL-1ra Regulation in RANKL-Induced Osteoclast Differentiation. To clarify whether the presence of DCR3 in RANKL-induced osteoclast differentiation was involved in IL-1α/IL-1ra regulation, we tested the expression levels of IL-1α and IL-1ra RNA using RT-PCR and QPCR in RAW264.7 cells and BMMs. The results showed that IL-1α mRNA was elevated within 6 hours after RANKL plus DCR3 stimulation in BMMs (Figures 2(a) and 2(b)) and RAW264.7 cells (sFigures 2A and 2C). Furthermore, the mRNA of intracellular IL-1ra (icIL-1ra) and secretory

(a)
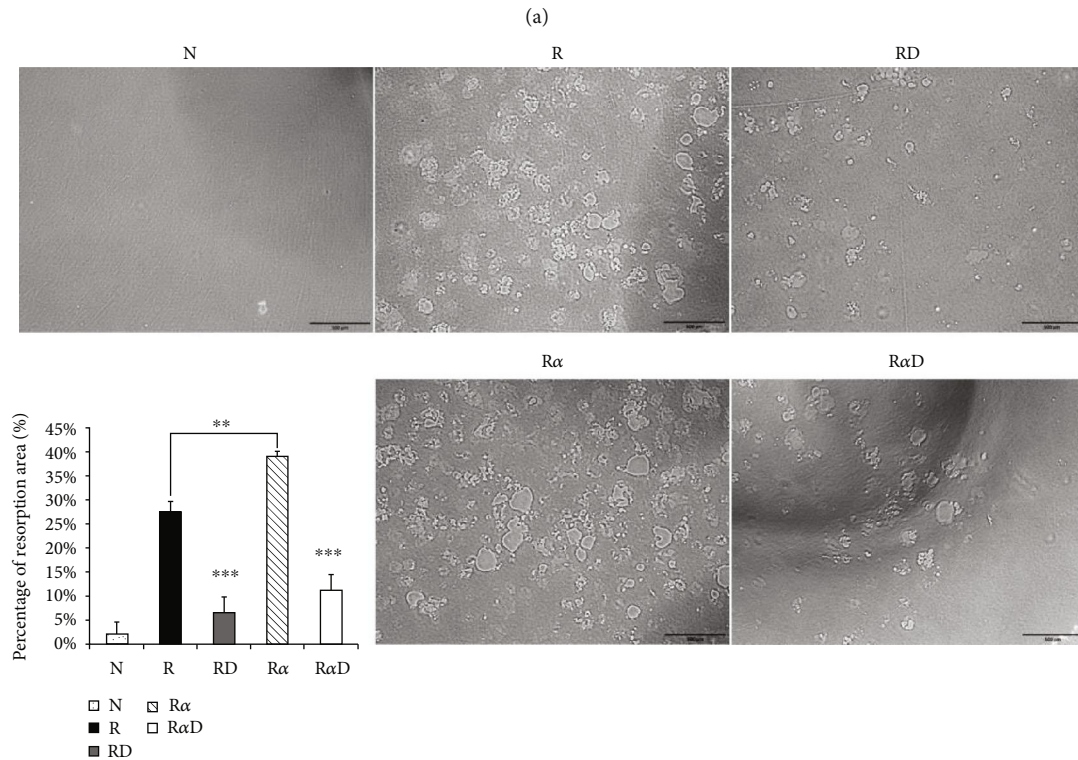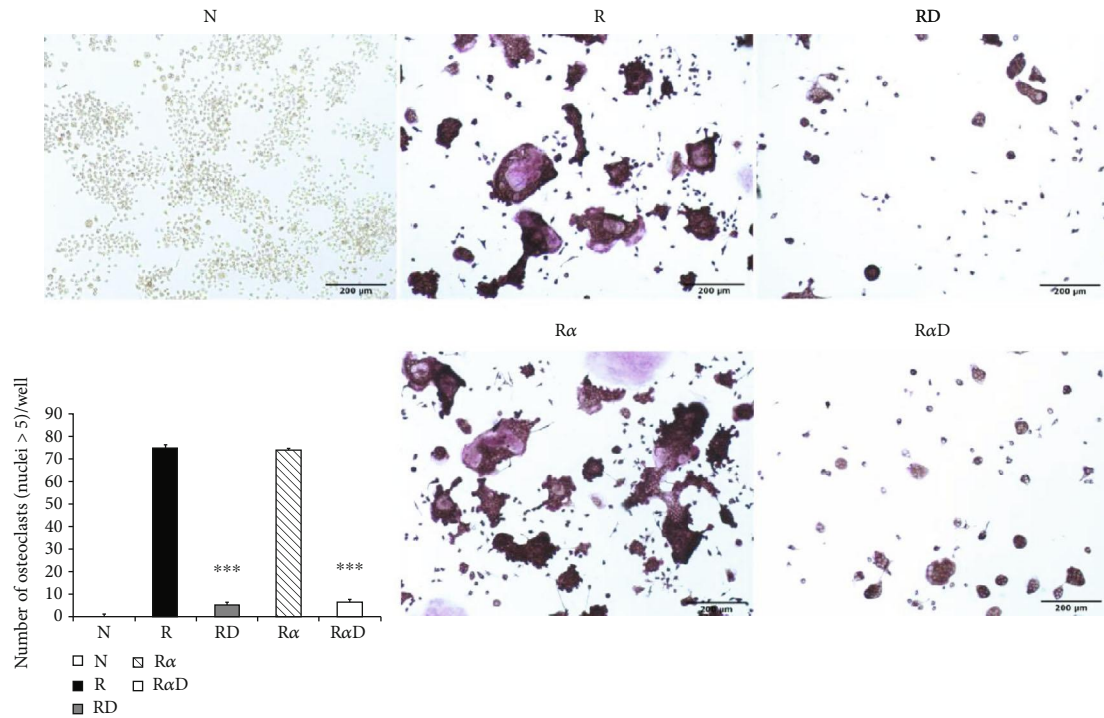
(b)

Figure 1: Effects of DCR3 on RANKL- plus IL-1α-induced osteoclast differentiation and function. (a) RAW264.7 cells were treated with DCR3 (10 μg/ml) in the presence of RANKL (50 ng/ml) or RANKL plus IL-1α (50 ng/ml) for 5 days. After incubation, the cells were fixed and stained for TRAP, and TRAP$^+$ multinucleated RAW264.7 cells containing more than five nuclei were counted as multinucleated osteoclasts. (b) RAW264.7 cells were seeded on dentine slices as described in the Materials and Methods. After being incubated for 5 days, the dentine slices were recovered from the culture and were subjected to a pit formation assay to visualize resorption. The percentages of the resorbed areas were determined using the NIH Image software. Data are presented as means ± SD of more than four slices and means ± SD of more than three cultures (N: RAW264.7 cells; R: RANKL; RD: RANKL+DCR3; Rα: RANKL+IL-1α; RαD: RANKL+ IL-1α+DCR3; $^{**}P < 0.01$ and $^{***}P < 0.001$).
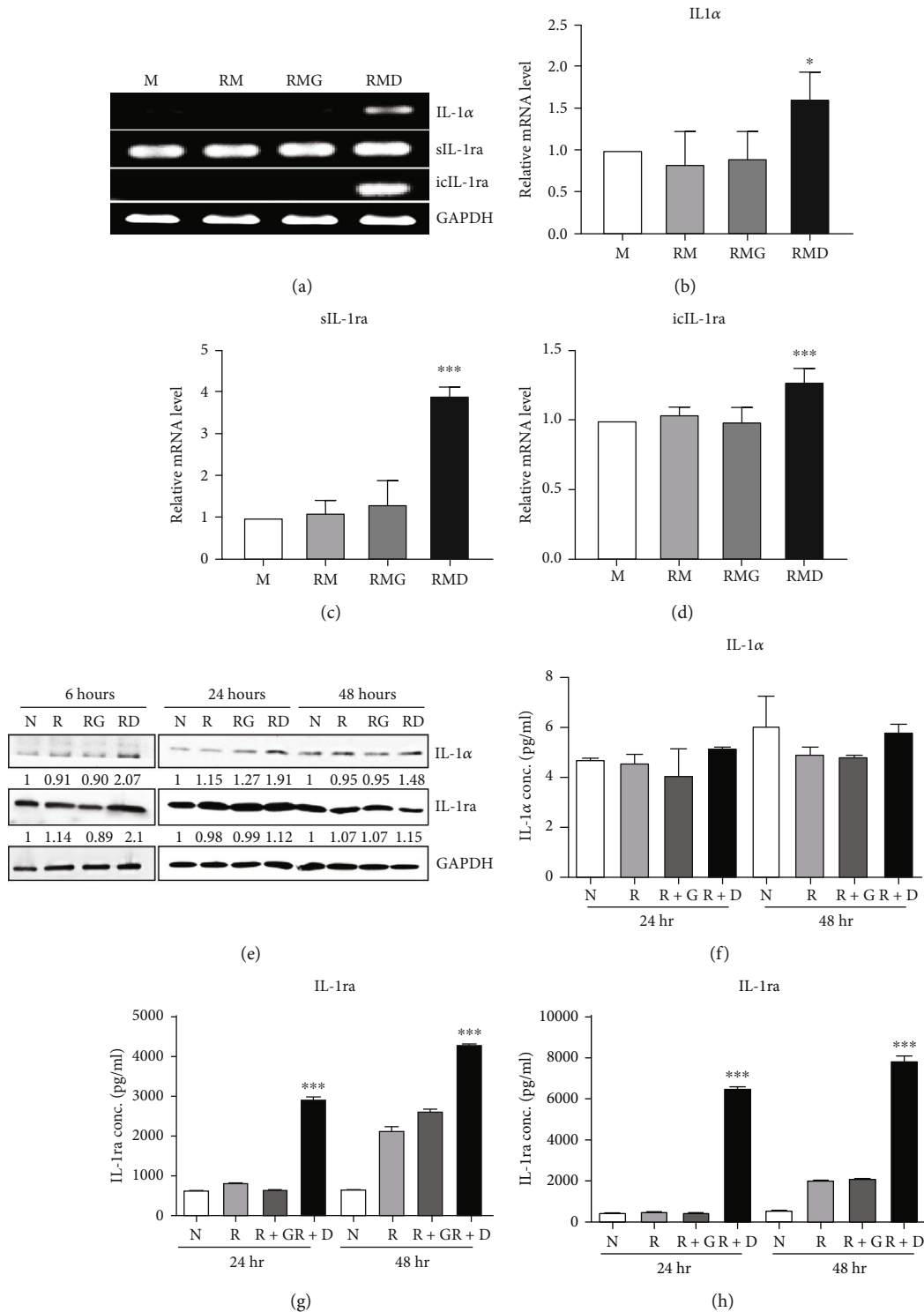
FIGURE 2: Effects of DCR3 on IL-1α and IL-1ra regulation on RANKL-induced osteoclast differentiation. (a–d) BMM cells were seeded at a density of 2×10^5 cells/well in a 24-well plate and treated with 10 μg/ml of DCR3 or IgG control in the presence of RANKL and M-CSF. After 6 hours of incubation, total RNA was isolated, and 1 μg of total RNA was used to reverse transcribe cDNA. Mouse IL-1α, sIL-1ra, and icIL-1ra were detected by RT-PCR (a) and QPCR (b–d). (e) RAW264.7 cells were treated with 10 μg/ml DCR3 or IgG in the presence of RANKL (50 ng/ml) stimulation for 6, 24, or 48 hours. Cell extracts were analyzed by immunoblotting assay. Equal amounts of protein were loaded in each lane as demonstrated by the level of GAPDH. (f) Supernatants at 24 or 48 hours were analyzed by IL-1α ELISA. Cell extracts (g) and supernatants (h) at 24 or 48 hours were analyzed by IL-1ra ELISA. A representative result of at least three independent experiments is shown (M: BMM cells+MCSF; RM: RANKL+MCSF; RMG: RANKL+MCSF+IgG; RMD: RANKL+MCSF+DCR3; N: RAW264.7 cells; R: RANKL; RG or R+G: RANKL+IgG; RD or R+D: RANKL+DCR3; ***$P < 0.001$).

IL-1ra (sIL-1ra) were also elevated at 6 hours after RANKL plus DCR3 stimulation in BMM (Figures 2(a), 2(c), and 2(d)) and RAW264.7 cells (sFigures 2B, 2D, and 2E). We further analyzed IL-1α and IL-1ra protein expression during osteoclast differentiation. Our results showed that the expression level of IL-1α significantly increased in the cell lysate at 6 hours in the early phase (Figure 2(e) and sFigure 3) but not in the supernatant (Figure 2(f)). The IL-1ra levels dramatically increased in the cells and supernatants in the DCR3-treated group at 24 and 48 hours (Figures 2(g), 2(h), and sFigure 3).

3.3. Effects of DCR3 on Reactive Oxygen Species and IL-1α Localization during Osteoclast Differentiation. In previous studies, IL-1α has been shown to be upregulated in ER-stressed macrophages and localized to the nucleus in apoptotic cells [31, 32]. To further clarify whether IL-1α was induced by DCR3 in ER-stressed apoptotic cells during osteoclastogenesis, we used an immunofluorescence stain to detect the level and distribution of IL-1α in each group 6 hours after DCR3 treatment. Our results showed that IL-1α accumulated in the endoplasmic reticulum of cells concurrently treated with RANKL and DCR3 (Figure 3(a)). Moreover, previous studies have shown that IL-1α and IL-1ra are markers of sterile inflammation in hypoxia/ROS-induced cell death [33, 34]. To understand whether DCR3 was involved in hypoxia/ROS-induced cell death in RANKL-induced osteoclast differentiation, we tested the expression levels of ROS in RAW264.7 cells. Interestingly, the results showed that the ROS levels were significantly increased by two-fold in the DCR3-treated group compared to the levels in groups treated with RANKL or with RANKL plus an IgG control (Figure 3(b)).

3.4. Effects of DCR3 on the Mechanisms of Apoptosis during Osteoclast Differentiation. Our previous work found that DCR3 enhances cell apoptosis in preosteoclasts by inducing Fas ligand expression. Here, we found that this phenomenon also occurred under IL-1α treatment concurrent with DCR3 treatment during RANKL-induced osteoclast differentiation (Figures 4(a) and 4(b)). Importantly, previous studies have reported that IRAK4 activation is a crucial process in inflammatory arthritis and participates in the Fas/FasL system induction of cytokine production and apoptosis in macrophages [35, 36]. Based on previous findings, we further investigated whether DCR3 was involved in the Fas/FasL induction of IRAK4 kinase activation during osteoclastogenesis in RAW264.7 cells. Surprisingly, the results indicated that the IRAK4 signal in RANKL-induced osteoclastogenesis was activated by DCR3 (Figure 4(c)).

4. Discussion

The present study is the first publication to find that DCR3 suppresses RANKL- plus IL-1α-induced osteoclastogenesis. The inhibitory effect of DCR3 was involved in the hypoxia/ROS- and IL-1α/IL-1ra-induced cell death signalling pathway. The first study of DCR3 in osteoclastogenesis was published by Yang et al., and they found that DCR3 itself,

without RANKL stimulation, induces osteoclast formation, bypassing the NF-κB signalling pathway, and induces TNFα expression [29]. However, another study by Tai et al. found that macrophage-specific CD68 promoter-driven DCR3 overexpression in transgenic mice strongly induces tumour-associated macrophages and IL-1ra and IL-10 expression; reduces proinflammatory cytokines (TNFα and IL-6); and does not affect MMP2, MMP9, or bone development in mice [27]. The controversial results concerning the role of DCR3 in macrophage differentiation and the expression of cytokines, such as TNFα in vitro and in vivo, raised our curiosity. Hence, we repeated the same experiment in vitro by using the DCR3 recombinant protein and full-length gene transient transfection. We found that DCR3 suppressed osteoclast formation in vitro and attenuated collagen-induced arthritis in a mouse model in vivo [25, 26]. In addition, the suppressive effect of DCR3 on osteoclastogenesis was through Fas ligand expression and intrinsic mitochondria-induced cell apoptosis [26]. However, there are no studies discussing the regulatory function of DCR3 on IL-1α/IL-1ra in osteoclastogenesis.

The IL-1α cytokine has complicated and multiregulatory functions in different cell types. IL-1α and IL-1ra counterbalance each other in keratinocytes. In osteoclasts, IL-1α activates several signalling cascades, including the Akt, ERK, JNK, and NF-κB pathways [7]. IL-1α also acts in an autocrine manner in osteoclast formation and maintains osteoclast survival [37, 38]. Downregulation of IL-1α/β by knockout mice enhances bone mass [39]. Moreover, sterile inflammation proceeds via the IL-1α hypoxia/ROS pathway and regulates cell death [33, 34]. However, in vivo cell death for tissue repair and the acute monocyte response to cell death are much less dependent on the IL-1R-MyD88 pathway [40]. Hence, the biological function of IL-1α in monocyte/macrophage lineage cells may benefit cell survival and maintain tissue-specific macrophage functions, such as osteoclast processing. In addition, the cell death pathway of the IL-1α-induced IL-1R-MyD88 pathway may be independent in macrophages or osteoclasts. In our study, we found that DCR3 activated endogenous osteoclast IL-1α expression and subsequently induced IL-1ra expression like the counterregulated function in keratinocytes. Moreover, two isoforms of IL-1ra have been identified, and when intracellular IL-1ra is released during cell apoptosis it has a function equivalent to that of secreted IL-1ra [41, 42]. Our findings demonstrated that DCR3 induced abundant icIL-1ra expression in preosteoclasts. In addition, the dramatic increase of icIL-1ra was accompanied by the suppression of osteoclastogenesis and induction of preosteoclast cell death.

DCR3 and its ligands, FASLG, LIGHT, and TL1A, are highly expressed in many inflammatory osteolytic diseases and are involved in osteoclastogenesis and cell death [43–46]. Our previous study demonstrated that DCR3 increases apoptosis of osteoclasts by increasing the level of the major ligand FASLG. Moreover, by connecting the Fas ligand with mitochondrial cell death, ROS have been shown to be critical factors in regulating the Fas death system in macrophages [47]. Although many studies have reported that ROS plays a critical role in the maintenance of macrophage phagocytosis ability and osteoclast differentiation [5, 48], ROS still
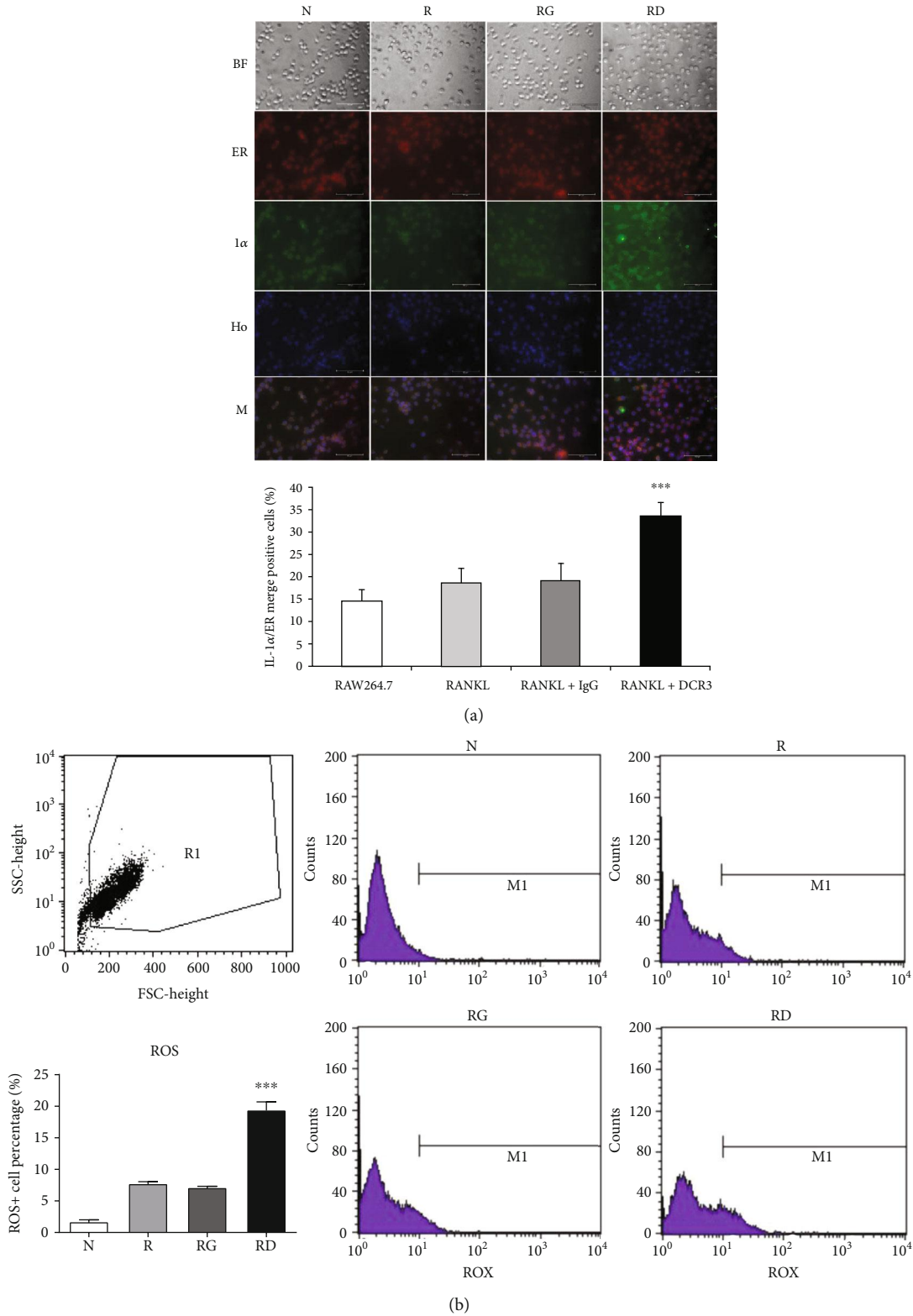
(a)

(b)

FIGURE 3: Effects of DCR3 on IL-1α protein localization and ROS expression in RANKL-induced osteoclast differentiation. RAW264.7 cells were treated with DCR3 or IgG in the presence of RANKL stimulation for 6 hours. After the time indicated, the cells were stained with an anti-IL-1α antibody (green), endoplasmic reticulum (red), and Hoechst dye (blue) or with a ROX detection kit. (a) The localization of IL-1α was compared in merged images for each group. (b) The ROS levels in each group were evaluated by flow cytometry. A representative result of at least three independent experiments is shown (BF: bright field; ER: endoplasmic reticulum staining; 1α: IL-1α staining; Ho: nuclear staining; M: merge image of ER, 1α, and Ho; N: RAW264.7 cells; R: RANKL; RG: RANKL+IgG; RD: RANKL+DCR3; ***$P < 0.001$).
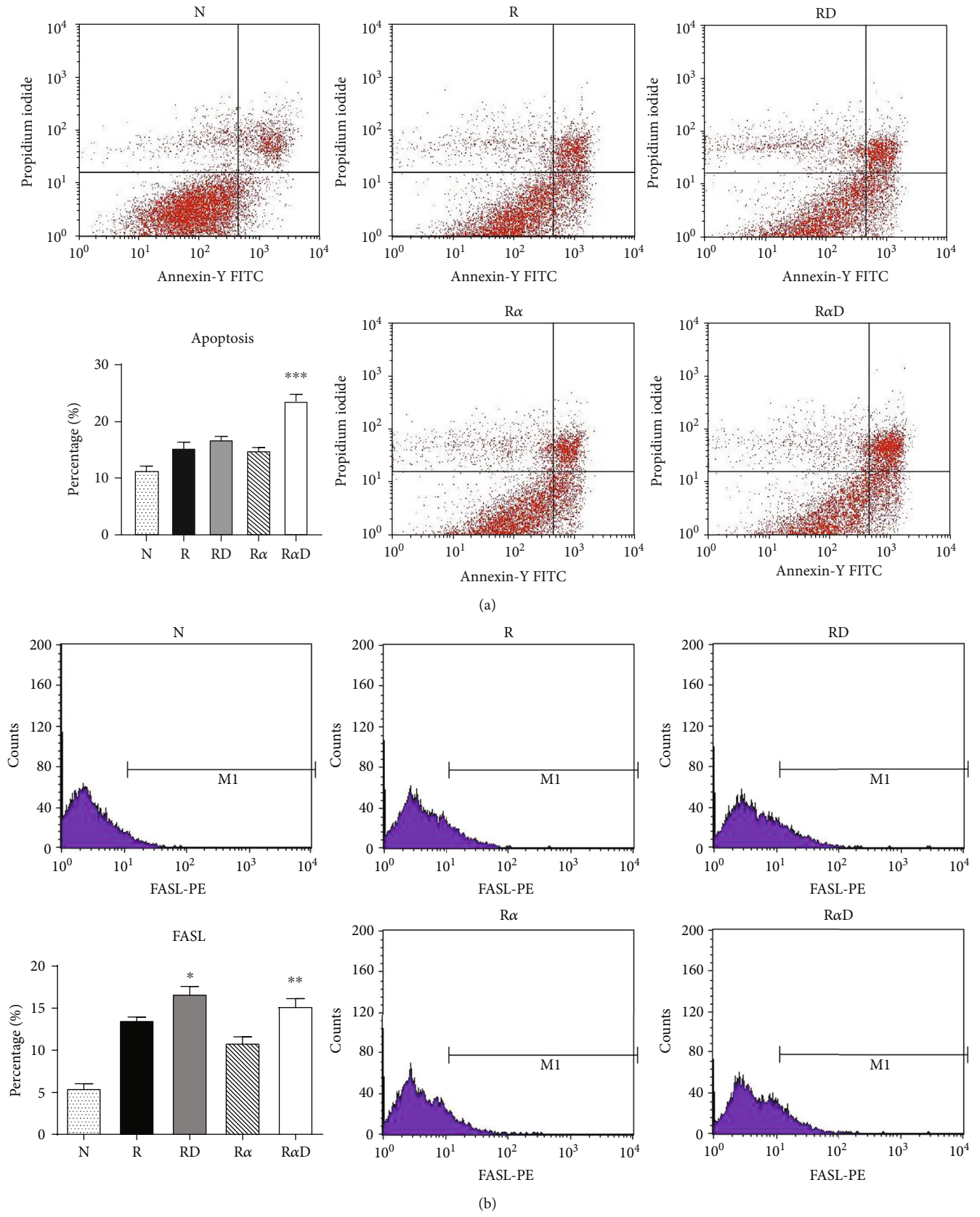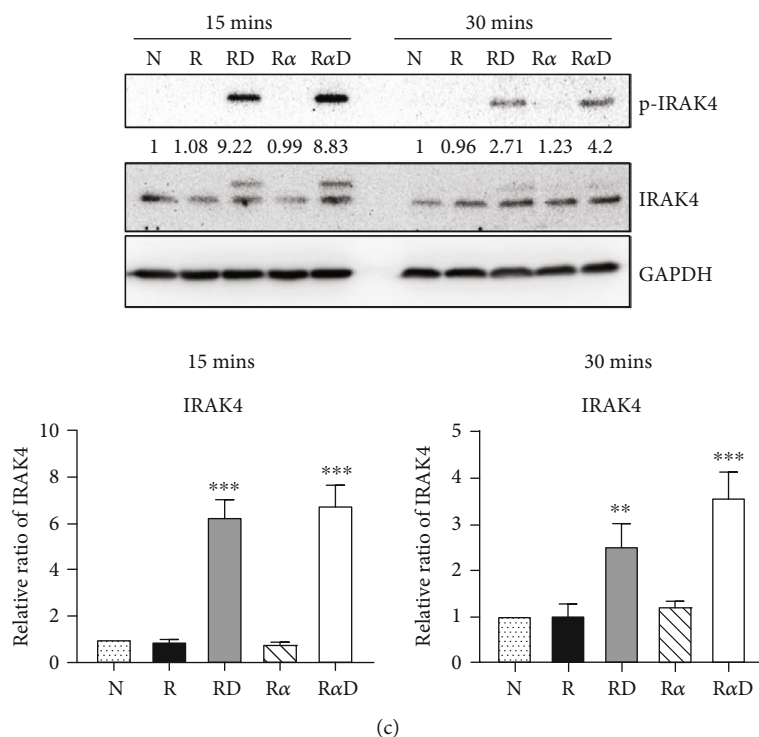
(a)

(b)

FIGURE 4: Continued.

FIGURE 4: Effects of DCR3 on cell apoptosis and interleukin-1-associated kinase activation in osteoclasts. RAW264.7 cells were treated for 48 hours with or without 10 μg/ml of DCR3 in the presence of RANKL or RANKL plus IL-1α. After incubation, cells were harvested for staining with (a) Annexin V and PI to evaluate the percentage of cell apoptosis or with (b) anti-Fas ligand to evaluate death ligand expression. (c) RAW264.7 cells were serum-starved overnight and treated with DCR3 in the presence of RANKL or RANKL plus IL-1α for 15 or 30 minutes. Cell extracts were analyzed by western blot analysis using antibodies specifically directed against the phosphorylated forms of IRAK4, compared to data obtained with antibodies directed against the unphosphorylated states of the kinases. Equal amounts of protein were loaded in each lane as demonstrated by the level of GAPDH. The expression ratio of phosphorylated/nonphosphorylated IRAK4 was quantified and normalized to the GAPDH. A representative result of at least three independent experiments is shown (N: RAW264.7 cells; R: RANKL; Rα: RANKL+IL-1α; RD: RANKL+DCR3; RαD: RANKL+IL-1α+DCR3; $^*P < 0.05$, $^{**}P < 0.01$, and $^{***}P < 0.001$).

guided the intrinsic endoplasmic reticulum (ER) stress-induced apoptosis in macrophages [49]. Previous studies have also demonstrated that ROS regulates IL-1α and IL-1ra expression in hypoxia-induced cell death [33, 34]. The IRAK4 kinase also participates in the Fas/FasL system and mediated apoptosis in macrophages [38]. Here, we found that DCR3 enhanced the ROS levels as well as IL-1α and IL-1ra expression during osteoclastogenesis. The mechanism of cell death was involved in linking DCR3 with the Fas/FasL system-induced activation of IRAK4. This function resorted to DCR3 because it might bond with its natural cell surface ligand, FasL, internalized into the macrophage, and it might stop the FasL-transduced osteoclastogenesis signalling and put macrophages forward to ROS-ER stress cell death. In addition, hypoxia-induced ROS have been reported to be involved in tumour formation [50]. In this regard, DCR3 might suppress osteoclast formation on the one hand, but could promote tumour-like osteolytic disease formation, such as rheumatoid arthritis, on the other.

In conclusion, we provide the first evidence that DCR3 exhibits inhibitory effects on RANKL- plus IL-1α-stimulated osteoclastogenesis as well as on pit formation. The molecular mechanisms of this inhibition involve intracellular ROS accumulation, IRAK4 kinase activation, and ROS induction

of Fas ligand, IL-1α, and icIL-1ra expression. The blockage of RANKL- plus IL-1α-stimulated osteoclastogenesis by DCR3 leads to preosteoclast cell death. In summary, our study may be used to determine the possible molecular mechanisms of DCR3 in osteoclastogenesis and may reveal DCR3 as a potential therapeutic agent that is beneficial for the treatment of inflammatory bone disorder diseases, such as gingivitis, which are involved in IL-1α/IL-1ra imbalances.

Data Availability

The data used to support the findings of this study are available from the corresponding author upon request.

Conflicts of Interest

The authors have declared no conflicts of interest.

Acknowledgments

Supplementary Materials

sFigure 1: effects of DCR3 on RANKL- plus IL-1α-induced osteoclast differentiation in BMMs. sFigure 2: effects of DCR3 on IL-1α and IL-1ra mRNA regulation in RANKL-induced osteoclast differentiation. sFigure 3: effects of DCR3 on IL-1α and IL-1ra protein expression on RANKL-induced osteoclast differentiation. Supplementary Table 1: list of murine PCR primers. (*Supplementary Materials*)

References

[1] T. Wada, T. Nakashima, N. Hiroshi, and J. M. Penninger, "RANKL-RANK signaling in osteoclastogenesis and bone disease," *Trends in Molecular Medicine*, vol. 12, no. 1, pp. 17–25, 2006.

[2] M. A. Lomaga, W.-C. Yeh, I. Sarosi et al., "TRAF6 deficiency results in osteopetrosis and defective interleukin-1, CD40, and LPS signaling," *Genes & Development*, vol. 13, no. 8, pp. 1015–1024, 1999.

[3] W. J. Boyle, W. S. Simonet, and D. L. Lacey, "Osteoclast differentiation and activation," *Nature*, vol. 423, no. 6937, pp. 337–342, 2003.

[4] S. L. Teitelbaum and F. P. Ross, "Genetic regulation of osteoclast development and function," *Nature Reviews Genetics*, vol. 4, no. 8, pp. 638–649, 2003.

[5] N. K. Lee, Y. G. Choi, J. Y. Baik et al., "A crucial role for reactive oxygen species in RANKL-induced osteoclast differentiation," *Blood*, vol. 106, no. 3, pp. 852–859, 2005.

[6] H. Ha, H. Bok Kwak, S. Woong Lee et al., "Reactive oxygen species mediate RANK signaling in osteoclasts," *Experimental Cell Research*, vol. 301, no. 2, pp. 119–127, 2004.

[7] J. H. Kim, H. M. Jin, K. Kim et al., "The mechanism of osteoclast differentiation induced by IL-1," *Journal of Immunology*, vol. 183, no. 3, pp. 1862–1870, 2009.

[8] M. H. Schiff, "Role of interleukin 1 and interleukin 1 receptor antagonist in the mediation of rheumatoid arthritis," *Annals of the Rheumatic Diseases*, vol. 59, no. 90001, pp. 103i–1108, 2000.

[9] Y. Niki, H. Yamada, S. Seki et al., "Macrophage- and neutrophil-dominant arthritis in human IL-1α transgenic mice," *The Journal of Clinical Investigation*, vol. 107, no. 9, pp. 1127–1135, 2001.

[10] Y. Niki, H. Yamada, T. Kikuchi et al., "Membrane-associated IL-1 contributes to chronic synovitis and cartilage destruction in human IL-1 alpha transgenic mice," *Journal of Immunology*, vol. 172, no. 1, pp. 577–584, 2003.

[11] S. Wei, H. Kitaura, P. Zhou, F. P. Ross, and S. L. Teitelbaum, "IL-1 mediates TNF-induced osteoclastogenesis," *The Journal of Clinical Investigation*, vol. 115, no. 2, pp. 282–290, 2005.

[12] A. Ashkenazi, "Targeting death and decoy receptors of the tumour-necrosis factor superfamily," *Nature Reviews. Cancer*, vol. 2, no. 6, pp. 420–430, 2002.

[13] R. M. Pitti, S. A. Marsters, D. A. Lawrence et al., "Genomic amplification of a decoy receptor for Fas ligand in lung and colon cancer," *Nature*, vol. 396, no. 6712, pp. 699–703, 1998.

[14] K. Y. Yu, B. Kwon, J. Ni, Y. Zhai, R. Ebner, and B. S. Kwon, "A newly identified member of tumor necrosis factor receptor superfamily (TR6) suppresses LIGHT-mediated apoptosis," *The Journal of Biological Chemistry*, vol. 274, no. 20, pp. 13733–13736, 1999.

[15] T.-S. Migone, J. Zhang, X. Luo et al., "TL1A is a TNF-like ligand for DR3 and TR6/DcR3 and functions as a T cell costimulator," *Immunity*, vol. 16, no. 3, pp. 479–492, 2002.

[16] J. Zhang, T. W. Salcedo, X. Wan et al., "Modulation of T-cell responses to alloantigens by TR6/DcR3," *The Journal of Clinical Investigation*, vol. 107, no. 11, pp. 1459–1468, 2001.

[17] C. Bai, B. Connolly, M. L. Metzker et al., "Overexpression of M68/DcR3 in human gastrointestinal tract tumors independent of gene amplification and its location in a four-gene cluster," *Proceedings of the National Academy of Sciences of the United States of America*, vol. 97, no. 3, pp. 1230–1235, 2000.

[18] W. Roth, S. Isenmann, M. Nakamura et al., "Soluble decoy receptor 3 is expressed by malignant gliomas and suppresses CD95 ligand-induced apoptosis and chemotaxis," *Cancer Research*, vol. 61, no. 6, pp. 2759–2765, 2001.

[19] H. H. Sung, J. H. Juang, Y. C. Lin et al., "Transgenic expression of decoy receptor 3 protects islets from spontaneous and chemical-induced autoimmune destruction in nonobese diabetic mice," *The Journal of Experimental Medicine*, vol. 199, no. 8, pp. 1143–1151, 2004.

[20] S. M. Ka, H. K. Sytwu, D. M. Chang, S. L. Hsieh, P. Y. Tsai, and A. Chen, "Decoy receptor 3 ameliorates an autoimmune crescentic glomerulonephritis model in mice," *Journal of the American Society of Nephrology*, vol. 18, no. 9, pp. 2473–2485, 2007.

[21] A. M. Mueller, X. Pedre, S. Killian, M. David, and A. Steinbrecher, "The Decoy Receptor 3 (DcR3, TNFRSF6B) suppresses Th17 immune responses and is abundant in human cerebrospinal fluid," *Journal of Neuroimmunology*, vol. 209, no. 1-2, pp. 57–64, 2009.

[22] S. J. Chen, Y. L. Wang, J. H. Kao et al., "Decoy receptor 3 ameliorates experimental autoimmune encephalomyelitis by directly countering local inflammation and downregulating Th17 cells," *Molecular Immunology*, vol. 47, no. 2-3, pp. 567–574, 2009.

[23] Y. C. Chang, T. L. Hsu, H. H. Lin et al., "Modulation of macrophage differentiation and activation by decoy receptor 3," *Journal of Leukocyte Biology*, vol. 75, no. 3, pp. 486–494, 2004.

[24] S. F. Wu, T. M. Liu, Y. C. Lin et al., "Immunomodulatory effect of decoy receptor 3 on the differentiation and function of bone marrow-derived dendritic cells in nonobese diabetic mice: from regulatory mechanism to clinical implication," *Journal of Leukocyte Biology*, vol. 75, no. 2, pp. 293–306, 2004.

[25] C. P. Cheng, H. K. Sytwu, and D. M. Chang, "Decoy receptor 3 attenuates collagen-induced arthritis by modulating T cell activation and B cell expansion," *The Journal of Rheumatology*, vol. 38, no. 12, pp. 2522–2535, 2011.

[26] C. P. Cheng, M. J. Sheu, H. K. Sytwu, and D. M. Chang, "Decoy receptor 3 suppresses RANKL-induced osteoclastogenesis via down-regulating NFATc1 and enhancing cell apoptosis," *Rheumatology (Oxford)*, vol. 52, no. 4, pp. 609–622, 2013.

[27] S. K. Tai, H. C. Chang, K. L. Lan et al., "Decoy receptor 3 enhances tumor progression via induction of tumor-associated macrophages," *Journal of Immunology*, vol. 188, no. 5, pp. 2464–2471, 2012.

[28] J. B. Mee, C. Antonopoulos, S. Poole, T. S. Kupper, and R. W. Groves, "Counter-regulation of interleukin-1alpha (IL-1alpha) and IL-1 receptor antagonist in murine keratinocytes," *The Journal of Investigative Dermatology*, vol. 124, no. 6, pp. 1267–1274, 2005.

[29] C. R. Yang, J. H. Wang, S. L. Hsieh, S. M. Wang, T. L. Hsu, and W. W. Lin, "Decoy receptor 3 (DcR3) induces osteoclast formation from monocyte/macrophage lineage precursor cells," *Cell Death and Differentiation*, vol. 11, Suppl 1, pp. S97–107, 2004.

[30] Y. J. Peng, C. H. Lee, C. C. Wang, D. M. Salter, and H. S. Lee, "Pycnogenol attenuates the inflammatory and nitrosative stress on joint inflammation induced by urate crystals," *Free Radical Biology & Medicine*, vol. 52, no. 4, pp. 765–774, 2012.

[31] N. M. Luheshi, N. J. Rothwell, and D. Brough, "The dynamics and mechanisms of interleukin-1alpha and beta nuclear import," *Traffic*, vol. 10, no. 1, pp. 16–25, 2009.

[32] M. Kandel-Kfir, T. Almog, A. Shaish et al., "Interleukin-1α deficiency attenuates endoplasmic reticulum stress-induced liver damage and CHOP expression in mice," *Journal of Hepatology*, vol. 63, no. 4, pp. 926–933, 2015.

[33] G. Y. Chen and G. Nunez, "Sterile inflammation: sensing and reacting to damage," *Nature Reviews. Immunology*, vol. 10, no. 12, pp. 826–837, 2010.

[34] A. Naldini, A. Pucci, and F. Carraro, "Hypoxia induces the expression and release of interleukin 1 receptor antagonist in mitogen-activated mononuclear cells," *Cytokine*, vol. 13, no. 6, pp. 334–341, 2001.

[35] J. Qin, Z. Jiang, Y. Qian, J. L. Casanova, and X. Li, "IRAK4 kinase activity is redundant for interleukin-1 (IL-1) receptor-associated kinase phosphorylation and IL-1 responsiveness," *The Journal of Biological Chemistry*, vol. 279, no. 25, pp. 26748–26753, 2004.

[36] F. Wang, Z. Lu, M. Hawkes, H. Yang, K. C. Kain, and W. C. Liles, "Fas (CD95) induces rapid, TLR4/IRAK4-dependent release of pro-inflammatory HMGB1 from macrophages," *Journal of Inflammation*, vol. 7, no. 1, p. 30, 2010.

[37] N. Tani-Ishii, A. Tsunoda, T. Teranaka, and T. Umemoto, "Autocrine regulation of osteoclast formation and bone resorption by IL-1 alpha and TNF alpha," *Journal of Dental Research*, vol. 78, no. 10, pp. 1617–1623, 2016.

[38] Z. H. Lee, S. E. Lee, C. W. Kim et al., "IL-1alpha stimulation of osteoclast survival through the PI 3-kinase/Akt and ERK pathways," *Journal of Biochemistry*, vol. 131, no. 1, pp. 161–166, 2002.

[39] Y. M. Lee, N. Fujikado, H. Manaka, H. Yasuda, and Y. Iwakura, "IL-1 plays an important role in the bone metabolism under physiological conditions," *International Immunology*, vol. 22, no. 10, pp. 805–816, 2010.

[40] C. J. Chen, H. Kono, D. Golenbock, G. Reed, S. Akira, and K. L. Rock, "Identification of a key pathway required for the sterile inflammatory response triggered by dying cells," *Nature Medicine*, vol. 13, no. 7, pp. 851–856, 2007.

[41] C. Gabay, B. Porter, G. Fantuzzi, and W. P. Arend, "Mouse IL-1 receptor antagonist isoforms: complementary DNA cloning and protein expression of intracellular isoform and tissue distribution of secreted and intracellular IL-1 receptor antagonist in vivo," *Journal of Immunology*, vol. 159, no. 12, pp. 5905–5913, 1997.

[42] J. Y. Chwee, M. Khatoo, N. Y. J. Tan, and S. Gasser, "Apoptotic cells release IL1 receptor antagonist in response to genotoxic stress," *Cancer Immunology Research*, vol. 4, no. 4, pp. 294–302, 2016.

[43] J. R. Edwards, S. G. Sun, R. Locklin et al., "LIGHT (TNFSF14), a novel mediator of bone resorption, is elevated in rheumatoid arthritis," *Arthritis and Rheumatism*, vol. 54, no. 5, pp. 1451–1462, 2006.

[44] J. Zhang, X. Wang, H. Fahmi et al., "Role of TL1A in the pathogenesis of rheumatoid arthritis," *Journal of Immunology*, vol. 183, no. 8, pp. 5350–5357, 2009.

[45] W. U. Kim, S. K. Kwok, K. H. Hong et al., "Soluble Fas ligand inhibits angiogenesis in rheumatoid arthritis," *Arthritis Research & Therapy*, vol. 9, no. 2, p. R42, 2007.

[46] H. Park, Y. K. Jung, O. J. Park, Y. J. Lee, J. Y. Choi, and Y. Choi, "Interaction of Fas ligand and Fas expressed on osteoclast precursors increases osteoclastogenesis," *Journal of Immunology*, vol. 175, no. 11, pp. 7193–7201, 2005.

[47] D. Medan, L. Wang, D. Toledo et al., "Regulation of Fas (CD95)-induced apoptotic and necrotic cell death by reactive oxygen species in macrophages," *Journal of Cellular Physiology*, vol. 203, no. 1, pp. 78–84, 2005.

[48] H. Y. Tan, N. Wang, S. Li, M. Hong, X. Wang, and Y. Feng, "The reactive oxygen species in macrophage polarization: reflecting its dual role in progression and treatment of human diseases," *Oxidative Medicine and Cellular Longevity*, vol. 2016, Article ID 2795090, 16 pages, 2016.

[49] Y. J. Lim, H. H. Choi, J. A. Choi et al., "Mycobacterium kansasii-induced death of murine macrophages involves endoplasmic reticulum stress responses mediated by reactive oxygen species generation or calpain activation," *Apoptosis*, vol. 18, no. 2, pp. 150–159, 2013.

[50] G. Y. Liou and P. Storz, "Reactive oxygen species in cancer," *Free Radical Research*, vol. 44, no. 5, pp. 479–496, 2010.

RESEARCH ARTICLE

THE FASEB JOURNAL

Astaxanthin attenuates joint inflammation induced by monosodium urate crystals

Yi-Jen Peng[1] | Jeng-Wei Lu[2] | Feng-Cheng Liu[3] | Chian-Her Lee[4] | Herng-Sheng Lee[5] | Yi-Jung Ho[6] | Tsung-Hsun Hsieh[1] | Chia-Chun Wu[7] | Chih-Chien Wang[7]

[1]Department of Pathology, Tri-Service General Hospital, National Defense Medical Center, Taipei, Taiwan

[2]Department of Biological Sciences, National University of Singapore, Singapore, Singapore

[3]Rheumatology/Immunology and Allergy, Department of Medicine, Tri-Service General Hospital, National Defense Medical Center, Taipei, Taiwan

[4]Department of Orthopedics, School of Medicine, College of Medicine, Taipei Medical University Hospital, Taipei Medical University, Taipei, Taiwan

[5]Department of Pathology and Laboratory Medicine, Kaohsiung Veterans General Hospital, Kaohsiung, Taiwan

[6]School of Pharmacy, Graduate Institute of Life Sciences, National Defense Medical Center, Taipei, Taiwan

[7]Department of Orthopedics, Tri-Service General Hospital, National Defense Medical Center, Taipei, Taiwan

Correspondence
Chih-Chien Wang, Department of Orthopedics, Tri-Service General Hospital, National Defense Medical Center, Taipei 114, Taiwan.
Email: tsghcc@gmail.com

Abstract

Gouty arthritis is the one of the most painful arthritis and is caused by an inflammatory reaction. This study investigated whether astaxanthin (AXT), which has documented anti-inflammatory and antioxidant properties, exhibits protective effects against monosodium urate (MSU) crystal-induced inflammation. Cell viability of J774A.1 murine macrophages was assessed by AXT dose-dependent incubation by MTT assays, and expression levels of iNOS and COX-2 proteins as well as secretion of IL-1β were also analyzed under MSU crystals stimulation with or without AXT treatment. The production of inflammatory mediators was found to significantly decrease with AXT treatment, and the formation of the inflammasome complex was also attenuated when cells were co-stimulated with MSU crystals and AXT. Furthermore, we found that expression of the MAPK pathway was downregulated in J774A.1 cells. AXT also inhibited the induction of COX-2 and IL-6 in human chondrocytes and synovial fibroblasts by western blots. Finally, an MSU crystal intra-articular injection rat model for gouty arthritis was utilized in which treatment groups received 5-daily intraperitoneal injections of AXT prior to MSU crystal stimulation, or once intra-articular injections of AXT following MSU crystal stimulation for 6 hours. Results of synovitis score analysis revealed that inflammation was significantly attenuated in the group which received intraperitoneal AXT injection prior to MSU crystal stimulation compared to the group which received MSU only. These results indicate that

AXT attenuates the effects of MSU crystal-induced inflammation by suppressing the production of pro-inflammatory cytokines and inflammatory mediators. Our findings that the anti-inflammatory activities of AXT may be beneficial in the treatment of MSU crystal-induced arthritis.

KEYWORDS

astaxanthin, inflammasome, inflammatory, monosodium urate, optical density (od)

1 | INTRODUCTION

Gouty arthritis is one of the most painful arthritis and is caused by an inflammatory reaction that arises in response to the deposition of monosodium urate (MSU) crystals in articular joints. Gouty arthritis affects the bursal tissues of individuals with hyperuricemia, provoking robust inflammation, and unbearable pain.[1,2] Previous studies have reported that MSU crystals may upregulate gene expression of cyclooxygenase 2 (COX-2), interleukin 8 (IL-8), and inducible nitric oxide synthase (iNOS) in mononuclear cells and articular chondrocytes.[3,4] Data from our earlier research have indicated that the anti-inflammatory and anti-nitrosative activities of pycnogenol may be beneficial the treatment of MSU crystal-induced arthritis.[5]

Inflammasome activation induces the secretion of pro-inflammatory cytokines by macrophages, such as interleukin 1 beta (IL-1β).[6-8] One of the most intensively studied inflammasomes is the NLRP3 inflammasome, which contains a nucleotide-binding oligomerization domain, a leucine-rich repeat pyrin 3 domain, an NLRP3 sensor, an ASC adaptor, and a caspase-1 protease.[9]. NLRP3 inflammasomes play important roles in various inflammatory diseases. Once activated, NLRP3 upregulates cellular synthesis and maturation of several pro-inflammatory cytokines and chemokines, including IL-1β and IL-18, which result in inflammation against environmental or host-derived antigens. Gouty arthritis is one of the diseases of the NLRP3 inflammasome-mediated IL-1β production, triggered by the deposition of MSU crystals. Interruption of NLRP3-IL-1β axis is one of future therapeutic perspectives.[10]

Currently, most treatment modalities for the acute attack of gouty arthritis employ nonsteroidal anti-inflammatory drugs (NSAIDs), colchicine, corticosteroids, and intramuscular corticotropin. These drugs aim to provide rapid pain relief and minimize the damage caused by inflammatory responses. The urate-lowering drugs used to treat chronic gout are the uricosuric drugs which are xanthine oxidase inhibitors (allopurinol, oxipurinol, and febuxostat), and the uricolytic drugs (probenecid, benzbromarone, micronized fenofibrate, and losartan).[11-13] However, clinical use of these drugs is limited because they are not overly effective and they can lead to serious side effects, including gastrointestinal and cardiovascular problems. Therefore, there is a critical need to identify novel agents for the effective treatment of gouty arthritis.

Astaxanthin (AXT) is a natural carotenoid which exhibits anti-inflammatory and neuroprotective effects. Specifically, AXT is an oxycarotenoid that has been shown to effectively inhibit oxidative damage.[14,15] Recent studies have further reported that AXT can[1] increase immunoglobulin production in human cells in vitro,[2] enhance the response and function of mouse splenic lymphocytes, and[3] increase mitogen-induced blastogenesis and cytotoxic activity.[16-19] However, the therapeutic effects of AXT to gouty arthritis still need to be unraveled.

In this study, we aimed to identify potential mechanisms of AXT in the treatment of inflammatory arthritis. Determination of this mechanism has the potential to ameliorate MSU crystal-mediated arthritis and to elucidate how AXT affects synovial fibroblasts and articular chondrocytes both in vitro and in vivo. Finally, elucidating the signaling functions of AXT could be beneficial for the future development of therapeutics targeting inflammation.

2 | MATERIALS AND METHODS

2.1 | MSU crystal-induced inflammation in rat knee joints

Male Sprague-Dawley (SD) rats weighing 300 to 400 g were obtained from the National Applied Research Laboratories and the National Laboratory Animal Center (Taiwan). All experiments and animal treatment protocols were approved by the institutional animal care and use committee (IACUC) of the National Defense Medical Center, Taiwan (Protocol No. IACUC-18-147). Direct intra-articular (IA) injections into knee joints, containing 50 μL of 1 mg/mL MSU crystals were performed as described previously[20]; the contralateral knee joint acted as a control, which was IA injected with phosphate-buffered saline (PBS). Specifically, the treatment groups were as follows[1]: rats received daily intraperitoneal (IP) injections of AXT at 50 mg/kg for five days before receiving an IA injection of MSU crystals, or[2] an IA injection of MSU crystals, and then, 6 hours later, an IA injection containing 50 μL of 50 μM AXT.

In this MSU crystal-induced gouty arthritis rat model, 8 week-old rats were randomly divided into four groups: control (Saline treatment control), MSU injection only, prevention IP

injection of AXT for five days before MSU injection, and IA injection of AXT 6 h after injection of MSU. All experimental animals were sacrificed at 24h after receiving the last injection of MSU crystals or AXT treatment into rat knee joints. Knee joint tissues were then fixed in formalin and processed into paraffin wax. Wax sections were cut and subjected to hematoxylin and eosin (H&E) staining. Synovitis scores of H&E-stained slides were quantified based on a previous report.[20] Briefly, inflammation and edematous change were assigned as none, mild, moderate, or severe (score 0, 1, 2, and 3, respectively). The synovitis scores are sum of these two factors. The number of male SD rats was nine for each other experiments group.

2.2 | Cell culture and treatment

Human articular cartilage and synovial tissue samples were obtained, with consent and ethical approval (Tri-Service General Hospital, 1-102-05-091), from knee joints obtained at total knee replacement of patients with osteoarthritis. Articular hyaline cartilage and synovial tissues were aseptically removed from knee joints, respectively, cut into tiny pieces of $1 \times 1 \times 1$mm in size, and incubated with 10 mL of antimicrobial solution with PBS (500 IU/mL of penicillin/streptomycin) (Gibco Life Technology, Thermo Fisher Scientific Inc., IL, USA) for 1 hour before being washed with PBS and digested with 3 mg/mL of type H collagenase (Sigma-Aldrich Co., St. Louis, MO, USA) at 37°C for 3 hours. We first confirmed that samples had been digested by examining them under a light microscope, and we then collected cell suspensions using sterile Pastettes. After centrifugation at 1,000 rpm/157 rcf (g) for 10 minutes, supernatants were discarded and cell pellets were resuspended. Articular chondrocytes and synovial fibroblasts were then seeded at a density of 5×10^5 cells/mL in 60 mm petri dishes (Orange Scientific, Braine-I'Alleud, Belgium) that contained complete medium comprising 3 mL of DMEM-F12 medium supplemented with 10% of FBS (Sigma), 100 IU/mL of penicillin (Gibco), and 100 mg/mL of streptomycin (Gibco). These cells were maintained in a humidified 5% of CO_2 atmosphere at 37°C. Note that cells between passages 3-5 were used in subsequent experiments. For in vitro experiment and cell stimulation, J774A.1 cells incubated with various concentrations of AXT (10, 25, and 50 μM) for 1 hours, and then, cocultured with/without 0.2 mg/mL MSU crystals for 12 hours.

2.3 | MTT assay

Murine macrophage J774A.1 cells cultured in DMEM containing 10% of fetal bovine serum and 1% of penicillin/streptomycin were seeded in 96-well plates to 70% confluence. Cell viability was assessed by 3-4,5-dimethylthiazol-2-yl-2,5-diphenyl tetrazolium bromide (MTT) (Roche, Indianapolis, IN,

USA) according to the manufacturer's instructions. In brief, J774A.1 cells were seeded in 96-well plates at a density of 5×10^3 cells per well. After 24 hours of culturing, the cells were stimulated with various concentrations of AXT (10, 25, 50, and 100 μM) for an additional 12 hours. Following this incubation period, the medium was removed and 20 μL of MTT solution was then added to each well. Well plates were subsequently incubated at 37°C for 4 hours, and then, 200 mL of DMSO was added to each well under gentle shaking at 37°C for 15 minutes. Both of the no treatment and DMSO were as a control group, respectively.

Cell viability was assessed by measuring absorbance at 570 nm using a Microplate Absorbance Reader (Bio-Tek).

2.4 | Cytotoxicity assay

To evaluated cells culture medium lactate dehydrogenase (LDH) release, we using the CytoScan LDH Cytotoxicity Assay kit (G-Biosciences) according to the manufacturer's instructions. Cells were incubated with MSU, AXT, and AXT combined with MSU for 6 hours. Collected the culture medium 50 μL mixed with 50 μL LDH substrate in each well and incubated in room temperature keep in dark for 30 minutes. Then, added 50 μL stop solution, measured the optical density (OD) absorbance at 490 nm. The cytotoxicity % was calculated as 100× (Experimental OD_{490}—spontaneous OD_{490})/maximum OD_{490}.[21]

2.5 | Monosodium urate crystal synthesis

MSU crystals were prepared as previously described.[5] The resulting MSU crystals were dried at room temperature for five days after resuspended in PBS at a concentration of 24 mg/mL and sterilized in an autoclave.

2.6 | Protein extraction and western blotting

Cells and tissues were immediately washed with ice-cold PBS and lysed in situ for 15 minutes with ice-cold RIPA lysis buffer (Thermo Pierce, Thermo Fisher Scientific Inc., IL, USA) containing 100 μM Na_3VO_4 and 100X protease inhibitor cocktail (Thermo Pierce). Whole cell lysates were collected after being centrifuged at 14 000 rpm/30678 rcf (g) for 15 minutes, and then, protein concentrations were determined using the Lowry method. Equal amounts of protein were subsequently loaded onto 10% of SDS-polyacrylamide gel, and then, transferred to polyvinylidene fluoride (PVDF) membranes (Merck Millipore, Darmstadt, Germany). Membranes were blocked overnight at 4°C with 2% of bovine serum albumin (BSA) in TBST (12.5 mM of Tris/HCl, pH 7.6, 137 mM of NaCl, 0.1%
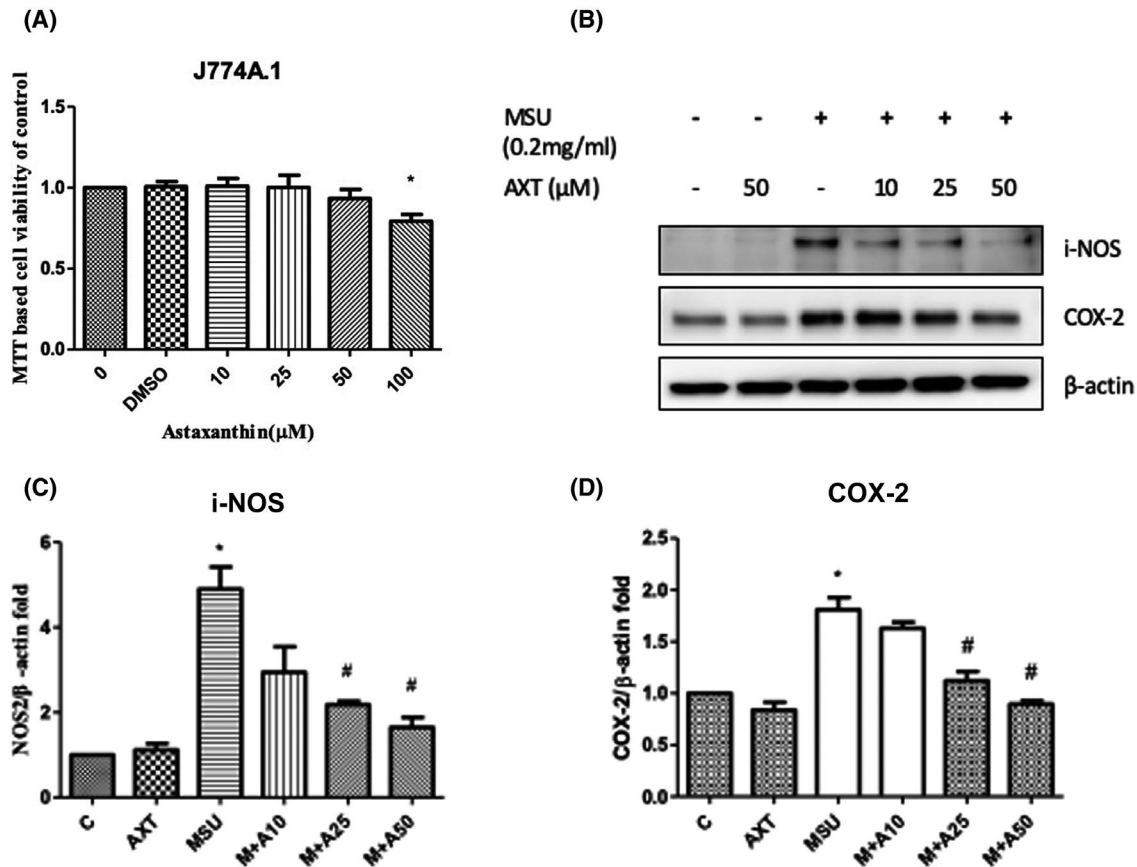
(A)

(B)

(C) i-NOS

(D) COX-2

FIGURE 1 Effects of AXT on cytotoxicity of MSU and viability of J774A.1 cells stimulated by MSU crystals according to iNOS and COX-2 expression levels. A, Cell viability was determined by an MTT assay 12 hours after J7741A.1 cells were exposed to AXT. Four different concentrations of AXT (10, 25, 50, and 100 μM) were evaluated. B, Representative gels showing cells incubated with AXT (10, 25, and 50 μM) for 1 hours, and then, coculture with MSU crystal (0.2 mg/mL) for 12 hours. Expression of iNOS and COX-2 proteins expression was detected by western immunoblotting with specific antibodies; β-actin served as internal control. C-D, Ratio of the intensities of iNOS and COX-2 proteins. Data are presented as mean ± SD. Significant differences with the control group were detected using ANOVA test with Dunnett post hoc test: MSU + AXT group (n = 6), *$P < .05$; MSU only group (n = 4), #$P < .05$, respectively

of Tween 20). After being washed three times with TBST, membranes were incubated with primary antibodies diluted in TBST. Blots were then washed with TBST three more times and incubated with HRP-labeled secondary antibodies for 1 hour at room temperature. Subsequently, membranes were washed extensively, and binding results were detected using the Enhanced Chemiluminescence plus Western blotting detection system (Merck Millipore), according to the manufacturer's instructions. Finally, membranes were scanned and analyzed by densitometry (VisionWorks LS, UVP, CA, USA), according to the manufacturer's instructions. The antibodies are listed in Supplementary Table 1.

2.7 | Statistical analysis

All data were averaged from at least three independent experiments. Quantitative data are presented as mean ± SD. ANOVA test with Dunnett post hoc test was chosen for

comparing two different treatment groups allowing for the nonsymmetrical distribution data. A P-value $< .05$ was considered statistically significant. All data were performed the normal distribution test using shapiro-wilk test and all results were nonsignificant ($P > .05$). All statistical analyses were conducted using SPSS Version 18.0 (SPSS Inc, Chicago, IL, USA), and results were presented using GraphPad Prism 5.0 (GraphPad software, CA, USA).

3 | RESULTS

3.1 | Quantitative analysis to assess cell viability and protective effects of AXT on inflammatory mediators in J774A.1 cells stimulated by MSU crystals

The effects of AXT on the growth and activity of J774A.1 cells were tested using MTT assays. We observed that, at a
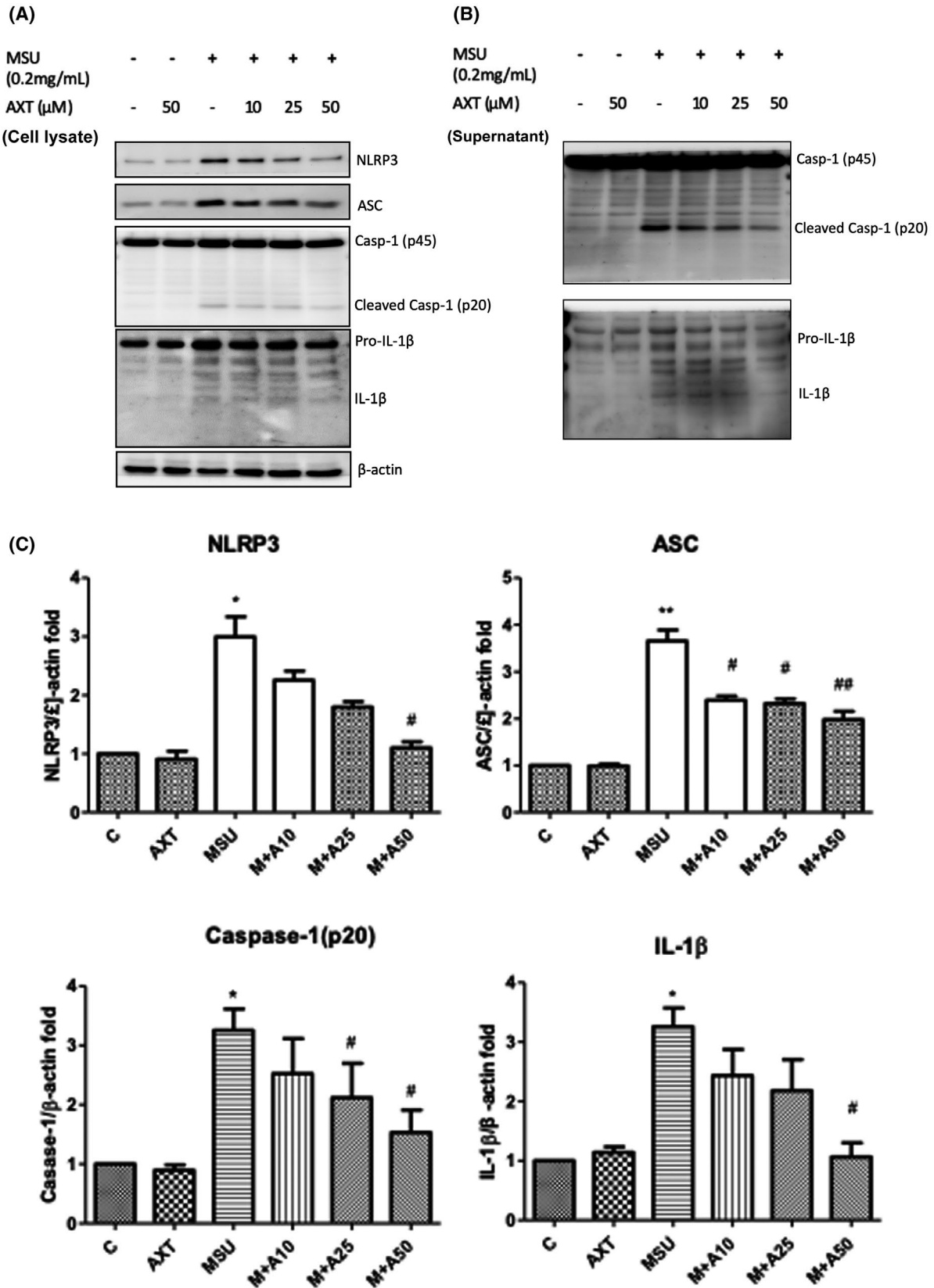
FIGURE 2 Effects of AXT on regulation of NLRP3, ASC, p45, and pro-IL-1β following stimulation with MSU crystals. A, Expression levels of NLRP3, ASC, p45, and pro-IL-1β were detected in cell lysates by Western blotting. B, Cell culture media were also collected and assayed for p20 and IL-1β secretion via Western blotting. C, The intensities of NLRP3, ASC, p45, and IL-1β protein expression levels were measured and normalized to β-actin. The secretion of the caspase-1 subunit p20 into the culture media of J774A.1 cells treated with MSU crystals or 10-50 μM AXT for 12 hours was assessed. Data are presented as mean ± SD. Significant differences were detected between the control and (1) the group that received AXT + MSU (n = 4; *P < .05; **P < .01) and (2) the group that received MSU crystals alone (n = 4; #P < .05; ##P < .01) using ANOVA test with Dunnett post hoc test, respectively

concentration of 10-50 µM, AXT did not affect cell viability after 12 hours of treatment (Figure 1A). Conversely, 100 µM AXT significantly decreased cell viability. AXT is normally considered to be nontoxic to cell growth. However, at a higher concentration, we found that AXT had a slight but significant effect on cell viability. As a result of this finding, we adopted a concentration of 50 µM AXT in subsequent experiments.

To determine the levels of inflammation-related proteins after MSU treatment, iNOS and COX-2 proteins were detected with specific antibodies by Western blotting (Figure 1B). The expression levels of iNOS and COX-2 did not significantly change with AXT (50 µM) treatment. Conversely, cells which were not treated with 50 µM AXT (ie, cells which only received 0.2 mg/mL of MSU) showed a significant increase in iNOS and COX-2 expression (4.89 ± 0.9-fold, $P = .01$; and 1.89 ± 0.20-fold, $P = .021$, respectively). Treatment with 10, 25, and 50 µM AXT for 1 hours, and then, coculture with 0.2 mg/mL of MSU crystal for 12 hours led to a decrease in the expression of inflammatory proteins compared with MSU crystal stimulation only. (Note that this decrease was inversely correlated with an increase in AXT concentration). Moreover, as shown in Figures 1C,D, when cells were treated 12 hours with 25 or 50 µM AXT, COX-2, and iNOS protein levels were significantly decreased compared to cells that received MSU crystal alone (1.64 ± 0.4-fold, $P = .04$; and 0.89 ± 0.05-fold, $P = .026$, respectively).

3.2 | AXT attenuates secretion of NLRP3 inflammasome complex in J774.1 cells stimulated by MSU crystals

Inflammasome activation results in the recruitment and activation of the NLRP3-ASC-caspase-1 (p45) complex. Caspase-1 is the key enzyme involved in the processing and cleavage of pro-IL-1β to form the biologically active IL-1β. Figures 2A,B show protein expression levels detected by western blotting method after J774.1 cells were pretreated with AXT for 1 h, and then, stimulated with MSU crystals for 12 h. We found that NLRP3, ASC, and caspase-1 expression levels did not change with AXT treatment. Conversely, when cells were stimulated with MSU but did not receive AXT treatment, NLRP3, ASC, and caspase-1 expression levels significantly increased (2.99 ± 0.59-fold, $P = .028$; 3.65 ± 0.40-fold, $P = .007$; and 3.25 ± 0.62-fold, $P = .02$, respectively). Cells that received both AXT (50 µM) and MSU (0.2 mg/mL) showed significantly decreased NLRP3, ASC, and caspase-1 expression levels compared to cells that received MSU crystals alone (1.1 ± 0.177-fold, $P = .049$; 1.98 ± 0.30-fold, $P = .01$; and 1.53 ± 0.38-fold, $P = .01$, respectively). To characterize the activation of IL-1β, cells were treated with MSU, and the presence of inactive pro-IL-1β and activate IL-1β was measured in cell culture supernatant. Pro-IL-1β did not significantly change when cells only received AXT treatment

(Figure 2B); however, pro-IL-1β increased significantly when cells were stimulated with MSU crystal (3.25 ± 0.54-fold, $P = .018$). As shown in Figure 2C, increasing the AXT concentration significantly reduced MSU crystal-induced IL-1β secretion (1.06 ± 0.41-fold, $P = .047$). On the contrary, based on the LDH releasing assay, AXT gave any detectable indication of cytotoxicity in J744.1A cells (Supplementary Figure 1). We has also provided these results of visualization of ASC specks effects of AXT were detected by treating J744.1A cells for 12 hours (Supplementary Figure 2).

3.3 | Effects of AXT on MSU crystal-induced inflammation in human articular chondrocytes and synovial fibroblasts

MSU crystals may directly deposit in the superficial layers of articular chondrocytes and synovial tissue within joint during acute gout attack. To determine a pathway by which AXT exerts anti-inflammatory effects on articular chondrocytes and synovial fibroblasts, the expression levels of COX-2 and IL-6 were examined (Figure 3A,B). The expression levels of COX-2 and IL-6 in synovial fibroblasts and articular chondrocytes stimulated by MSU did not significantly change with AXT treatment. However, when cells were stimulated by MSU but did not receive AXT treatment, expression levels of COX-2 proteins significantly increased in synovial fibroblasts and articular chondrocytes (4.33 ± 0.55-fold, $P = .009$; and 4.43 ± 1.95-fold, $P = .03$, respectively). Cells of pretreatment with AXT for 1 hours, and then, MSU crystals for 12 hours exhibited decreased expression of COX-2 proteins compared to cells stimulated by MSU alone (1.98 ± 0.37-fold, $P = .005$; and 1.62 ± 0.85-fold, $P = .02$, respectively). Moreover, when cells were stimulated with MSU crystals alone, expression levels of IL-6 proteins in synovial fibroblasts and articular chondrocytes also significantly increased (6.55 ± 1.99-fold, $P = .04$; and 3.87 ± 0.53-fold, $P = .01$, respectively). Cells treatment with AXT for 1 hours following MSU crystal-stimulation showed decreased expression of IL-6 proteins compared to cells stimulated by MSU crystals alone (1.82 ± 0.31-fold, $P = .04$; and 2.00 ± 0.26-fold, $P = .02$, respectively) (Figures 3C,D). Results pertaining to inflammatory effects in articular chondrocytes or synovial fibroblasts were similar.

3.4 | Effects of AXT on MSU crystal-induced MAP kinase activation in J774A.1 cells, articular chondrcoytes, and synovial fibroblasts

To determine a pathway by which AXT exerts anti-inflammatory effects, the activation of ERK1/2, p-38, and JNK was
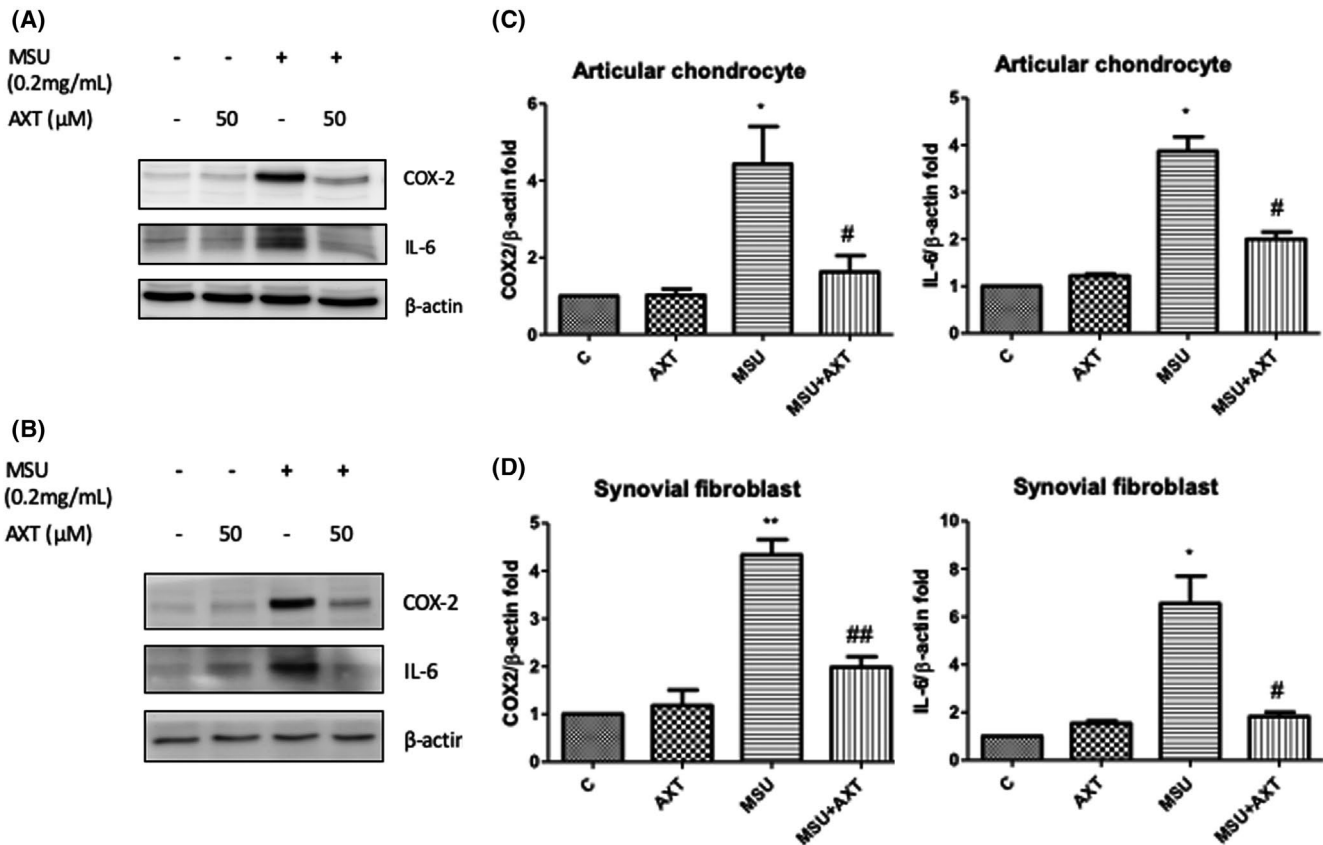
(A)

| MSU (0.2mg/mL) | - | - | + | + |
| AXT (μM) | - | 50 | - | 50 |

COX-2
IL-6
β-actin

(C)

(B)

| MSU (0.2mg/mL) | - | - | + | + |
| AXT (μM) | - | 50 | - | 50 |

COX-2
IL-6
β-actin

(D)

FIGURE 3 Effects of AXT in articular chondrocytes and synovial fibroblasts. A-B, Representative gels. C-D, Quantitative analysis of COX-2 and IL-6 expression in articular chondrocytes and synovial fibroblasts. Data are expressed as the mean ± SD. Significant differences were detected using ANOVA test with Dunnett post hoc test: n = 6, *P < .05; **P < .01 compared with the control group; and #P < .05; ##P < .01 *compared* with the MSU crystal group, respectively

examined by western immunoblotting (Figures. 4A,C,E). The phosphorylation of ERK1/2 peaked at 30 minutes, and phosphorylated p-38 and JNK, respectively, peaked at 30 minutes and 1 hours following stimulation with MSU crystals (0.2 mg/mL). In cells that were prestimulated with AXT and then, MSU crystal-stimulation for 30 minutes, the phosphorylation of ERK1/2 and p38 was found to be significantly attenuated compared to cells stimulated by MSU alone. Results pertaining to the phosphorylation of JNK proteins were similar to results pertaining to the phosphorylation of ERK1/2 and p38. In brief, cells pretreated with 50 μM AXT showed attenuated phosphorylation of ERK1/2, JNK, and p38 compared to cells stimulated by MSU crystals alone (Figures 4B,D,F).

3.5 | Effects of AXT on MSU crystal-induced inflammation in vivo

AXT is usually used orally as a nutritional product. Our hypothesis that astaxanthin has anti-inflammatory effects. In the previous study, the pharmacokinetic parameters of

astaxanthin presented dose-independent in oral administration that would make the therapeutic dose difficult to control.[22] Therefore, using IP pretreatment AXT to simulate the systemic effect caused by oral use of AXT would also effectively reduce errors and improve quantification.[23,24] A rat model with intra-articular injection of MSU crystals was used to determine the effects of AXT on gouty arthritis in vivo. Rats were divided into four groups: control (injected with PBS being used as a control), MSU crystals injection only, prevention intraperitoneal (IP) injection of AXT for five days before MSU crystals injection, and IA injection of AXT 6 h after injection of MSU crystals. All these rats were sacrificed 24 hours later after IA injection of AXT for 6 hours (n = 9 for each experiment group). Synovitis scores were used to standardize histopathological assessments of synovial membrane specimens (Figure 5A). All MSU treatment groups had significantly higher synovitis scores than did the control group. Histological analysis of the MSU crystal treatment groups revealed neutrophils-predominant inflammatory exudate in the joint space, inflammatory cells infiltration in the synovial tissue with mild synovial hyperplasia and edematous change. When preventative IP
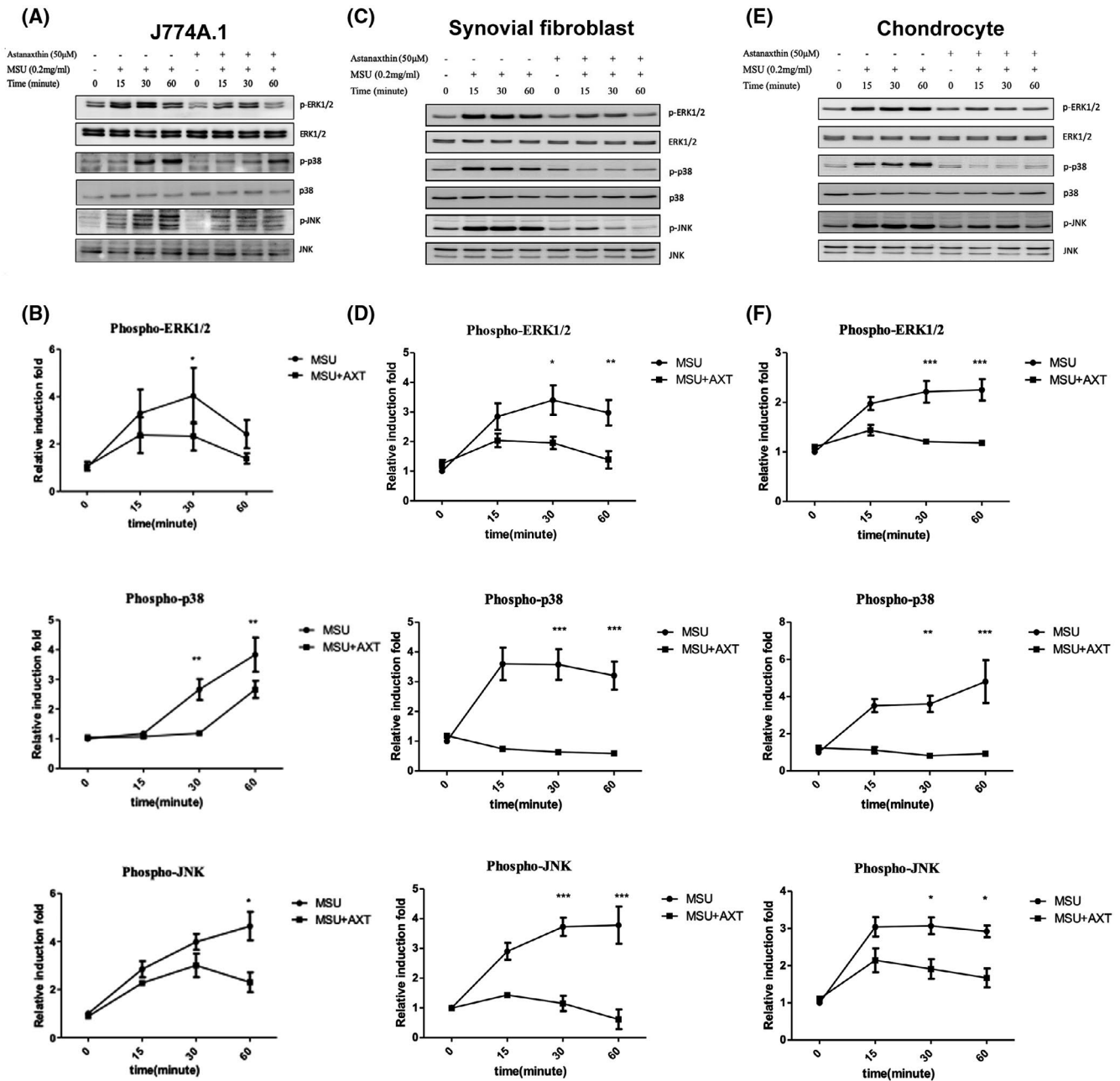
FIGURE 4 Effects of MSU crystals and AXT on cytosolic expression of ERK1/2, p38, and JNK phosphorylation levels in J774A.1 cell, synovial fibroblasts, and chondrocyte. Cells were incubated with the following: control, MSU crystals, AXT, or pretreatment of AXT n for 1 hours, and then, stimulated by MSU crystals for 15, 30, and 60 minutes. (A, C, and E) Representative gel. Ratio of the intensities of protein levels: (B, D, and F) phospho-ERK1/2 relative to ERK1/2, phospho-p38 relative to p38, and phospho-JNK relative to JNK. Data are expressed as the mean ± SD. Significant differences were detected between the control group and (1) the group that received MSU crystals (n = 4; *P < .05; **P < .01; ***P < .001) and (2) the group that received MSU crystals + AXT (n = 4; *P < .05; **P < .01; ***P < .001) using ANOVA test with Dunnett post hoc test, respectively

injections of AXT were administered for five days before MSU crystal injection, synovitis scores were significantly decreased compared to the group that received MSU alone. Similarly, in the group that received an IA injection of AXT 6 hours after MSU injection, synovitis scores were also significantly decreased compared to the group that received MSU alone (Figure 5B).

4 | DISCUSSION

In the current study, we investigated the therapeutic potential of AXT by assessing MSU crystal-stimulated inflammatory cytokines, and inflammatory proteins. MSU mainly stimulated synovial fibroblast to produce cytokines, causing an inflammatory response, and cytokines in turn affected the
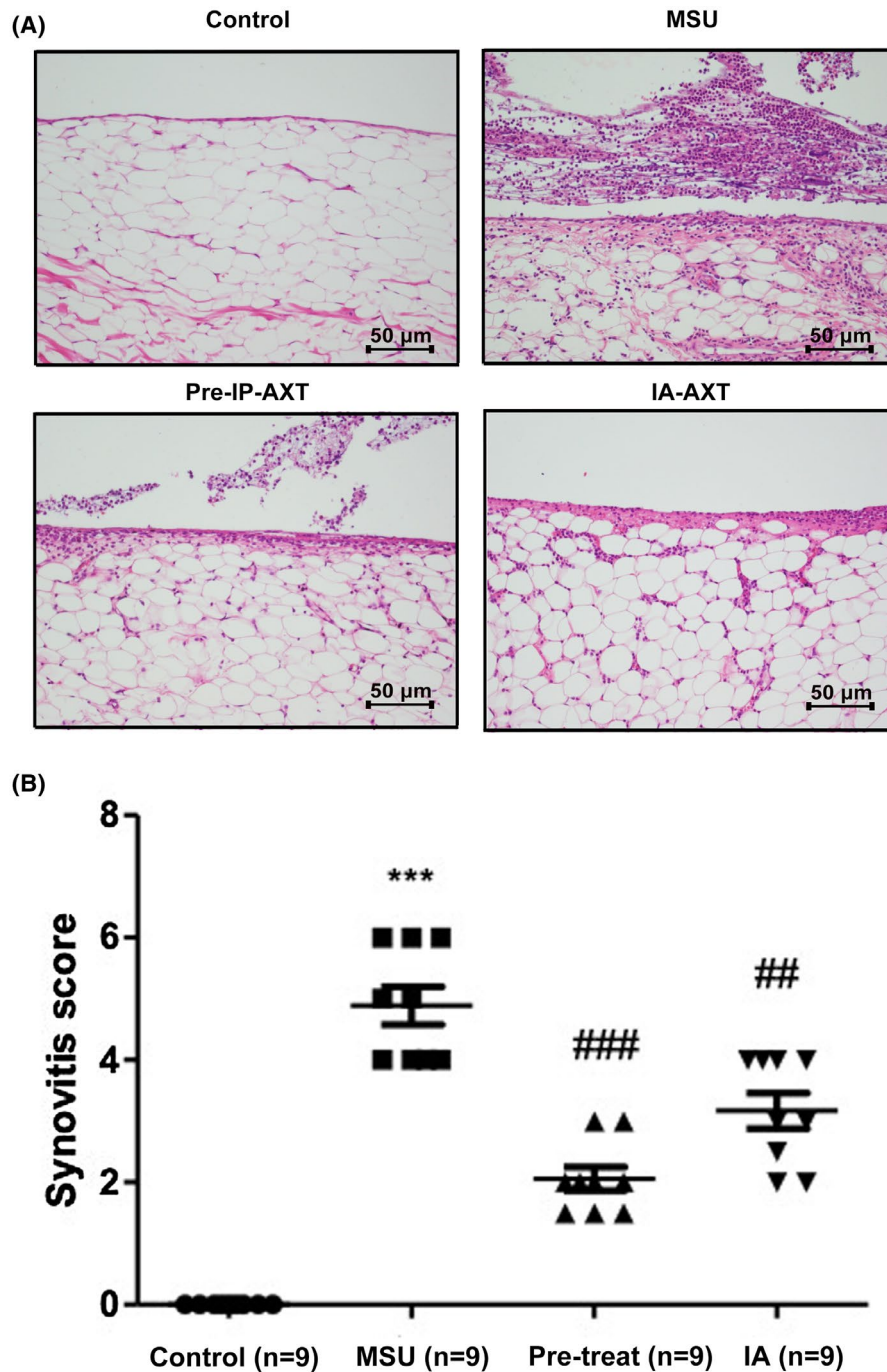
(A)

(B)

FIGURE 5 Histopathological analysis of rat knee joints from four treatment groups (n = 9 for each group). Effects of AXT in cartilage chondrocytes. A, Histopathological sections from four groups are shown. Histological analysis of the control group showed normal, MSU group showed neutrophils-predominant inflammatory exudate in the joint space, inflammatory cells infiltration in the synovial tissue with mild synovial hyperplasia and edematous change. With prevention IP injection or IA injection of AXT for five days or 6 h before MSU injection, respectively. The Pre-IP-AXT and IA-AXT groups showed reduced acute inflammation. B, Quantitative analysis of synovitis scores from four groups. Plotted data are expressed as mean ± SD. Significant differences were detected used ANOVA test with Dunnett post hoc test: n = 9, ***$P < .001$ compared with the control group and ##$P < .01$; ###$P < .001$ compared with the MSU crystal group, respectively

chondrocytes in the joint, causing damage, and finally triggering gouty arthritis. To further strengthen our understanding, we confirmed the anti-inflammatory effects of AXT in knee joints of rats in which inflammation was induced by MSU crystals. Specifically, we considered synovitis score, articular elastase, and pro-inflammatory cytokine levels. Our study demonstrated that AXT treatment suppressed the expression levels of inflammatory mediators (IL-1β, COX-2, ASC, the NLRP3 inflammasome, and caspase-1) induced by MSU crystals in J774A.1 cells, chondrocytes, and synovial fibroblasts.

According to previous studies, MSU can induce the secretion of inflammatory molecules in both human articular chondrocytes and synovial fibroblasts affected by gout and persistent hyperuricemia.[25] Microscopy research supported that MSU crystals presented in previously inflamed joints of the patients suffered from gout and persistent hyperuricemia. MSU crystals also observed at the bone damage erosion region by two-dimensional Dual-energy CT (DECT). This inflammatory stimulation can sustain an intense inflammatory response in the joint cavity, which is largely responsible for the pathology of gouty arthritis.[4,26] Several studies have also demonstrated that MSU crystal by macrophage can induce the formation of the NLRP3 inflammasomes, which can in turn cleave pro-IL-1β to the active IL-1β and subsequently activating caspase-1.[27] IL-1β is a pivotal inflammatory mediator that is able to induce the expression of a wide range of inflammatory mediators, including tumor necrosis factor alpha (TNF-α), IL-6, and IL-8. This can in turn induce an influx of neutrophils, which results in acute synovitis. MSU crystals and other danger signaling molecules are known to promote ROS generation inside cells.[28] To date, monotherapy including COX-inhibiting NSAIDs, systemic corticosteroids, or oral colchicine has been used as conventional first-line therapy to manage gouty arthritis. However, clinical use of this treatment modality is limited because it is not particularly effective and can lead to serious side effects.[29,30]

In the present study, we demonstrated that stimulation by MSU crystals leads to the production and expression of COX-2, NLRP3, and IL-1β in J774A.1 cells. Recent studies on gout pathogenesis have demonstrated that a single crystal of sodium urate can change the configuration of NLRP3, resulting in NLRP3 activation and the subsequent release of a large number of pro-inflammatory cytokines (ie, the initial pathogenesis of arthritis).[31,32] In the present study, we demonstrated that stimulation by MSU crystals leads to the production and expression of COX-2, NLRP3, and IL-1β in J774A.1 cells.

AXT, a xanthophyll carotenoid, has documented anti-inflammatory and antioxidant properties. Recent studies have demonstrated that AXT can enhance immune responses and also decrease inflammation as well as the levels of a DNA oxidative damage biomarker in young, healthy females.[33] AXT is a potent antioxidant that does not show pro-vitamin-A activity. This carotenoid may also be able to improve the chronic inflammation associated with oral lichen planus.[34] AXT is a more powerful scavenger of singlet oxygen and peroxyl radicals than are other carotenoids and b-carotenes due to its unique structure.[35] Positive biological responses to AXT have been reported in both in vitro and in vivo studies. For example, AXT was found to stimulate the proliferation of murine splenocytes and thymocytes in vitro and was also found to increase cytotoxic T lymphocyte activity in mice.[16,36] In the current study, protein levels of iNOS, COX-2, and NLRP3 markedly decreased following AXT treatment.

Nitric oxide (NO) is an inflammatory mediator produced by nitric oxide synthase (NOS).[37,38] NO is synthesized during the in vivo conversion of l-arginine to citrulline by NOS. NOS can be classified into three subfamilies according to the location of expression. Constitutive NOS is detected in neuronal tissues (nNOS) and vascular endothelial cells (eNOS), whereas iNOS is expressed in a variety of cell types. In addition, cyclooxygenase (COX, prostaglandin H2 synthase (PGHS)) is the key enzyme involved in the biosynthesis of prostaglandin from arachidonic acid.[39,40] COX-2 is an inducible enzyme involved in inflammatory events. Previous studies have shown that inflammatory signals can greatly enhance COX-2 expression. In the current research, we demonstrated that AXT treatment suppressed the production of iNOS and COX-2 in J774A.1 cells stimulated by MSU crystals. Since iNOS and COX-2 are needed for the formation of NO and PEG2, we speculate that the inhibition of NO and PEG2 production by AXT may be associated with the regulation of iNOS and COX-2 expression.

To determine whether the anti-inflammatory activities of AXT are due to inhibition of the MAPK pathway, we investigated the effects of AXT on ERK, p38, and JNK expression in J744A.1 cells, articular chondrocytes, and synovial fibroblasts stimulated by MSU crystals. Western blot analysis confirmed that, following MSU stimulation, AXT mainly exerts its anti-inflammatory effects by deactivating the MAPK pathway, which in turn inhibits the expression of COX-2 proteins and NLRP3 inflammasomes. Findings from this study suggest that AXT can attenuate the effects of inflammation induced by MSU crystals and can decrease the expression of ERK1/2, JNK, and p38 phosphorylation in J774A.1 cells, articular chondrocytes, and synovial fibroblasts. Our data also indicate that the MAPK pathway is a pivotal transcription factor for inflammatory signaling pathways.

To further strengthen our in vitro findings, we evaluated the potential of AXT to alleviate MSU crystal-induced inflammation in rat articular chondrocytes and synovial fibroblasts. Interestingly, our results demonstrated that AXT suppressed the expression of COX-2 and IL-6 in these rat cells. To standardize the histopathological assessment of the anti-inflammatory effects that AXT exerts on synovial inflammation, synovitis scores, which define the degree of immunological and inflammatory changes associated with synovitis and are also the standard for diagnostic histopathological scores, were employed to discriminate between chronic low-grade synovitis and chronic high-grade synovitis. A synovitis score between 1 and ≤4 indicates low-grade synovitis, and a score between ≥ 5 and 9 indicates high-grade synovitis. Our findings indicate that pretreatment with AXT via IP injection for five consecutive days before stimulation by MSU can significantly attenuate the effects of inflammation. Furthermore, administering AXT via IA injection 6 h after stimulation with MSU also significantly decreased

synovitis scores. Compared with the AXT via IA injection group, these results indicate that the synovitis score of the pretreatment AXT via IP injection group has decreased more, which means that the used of pretreatment AXT via IP injection (Simulated oral medication) could more effective than IA injection.

In conclusion, the present study demonstrated that AXT can attenuate the effects of MSU stimulation in chondrocytes by inhibiting the intracellular MAPK pathway, which in turn suppresses the production and expression of pro-inflammatory cytokines and inflammatory mediators. These anti-arthritic properties were further confirmed using a relevant animal model. The present study provides a rationale for the use of AXT as an anti-inflammation drug in the treatment of gouty arthritis. However, the mechanisms which underlie both the effects of AXT and the assembly and activation of NLRP3 inflammasomes still require further study.

ACKNOWLEDGMENTS

CONFLICT OF INTEREST

There are no conflicts of interest.

AUTHOR CONTRIBUTIONS

Y.-J. Peng and C.-C. Wang designed the project and experiments; Y.-J. Peng, J.-W. Lu, F.-C. Liu, C.-H. Lee, H.-S. Lee, and E.-J. Ho conducted the experiments; J.-W. Lu, F.-C. Liu, H.-S. Lee, E.-J. Ho, T.-H. Hsieh, C.-C. Wu, and C.-C. Wang performed data analysis and made the figures; Y.-J. Peng, J.-W. Lu. and C.-C. Wang wrote and revised the manuscript. All authors have read and agreed to the published version of the manuscript.

REFERENCES

1. Perez-Ruiz F, Dalbeth N, Bardin T. A review of uric acid, crystal deposition disease, and gout. *Adv Ther*. 2015;32:31-41.
2. Busso N, So A. Mechanisms of inflammation in gout. *Arthritis Res Ther*. 2010;12:206.
3. Nam JS, Jagga S, Sharma AR, et al. Anti-inflammatory effects of traditional mixed extract of medicinal herbs (MEMH) on monosodium urate crystal-induced gouty arthritis. *Chin J Nat Med*. 2017;15:561-575.
4. Dhanasekar C, Kalaiselvan S, Rasool M. Morin, a bioflavonoid suppresses monosodium urate crystal-induced inflammatory immune response in RAW 264.7 macrophages through the inhibition of inflammatory mediators, intracellular ROS levels and NF-kappaB activation. *PLoS ONE*. 2015;10:e0145093.
5. Peng YJ, Lee CH, Wang CC, Salter DM, Lee HS. Pycnogenol attenuates the inflammatory and nitrosative stress on joint inflammation induced by urate crystals. *Free Radic Biol Med*. 2012;52:765-774.
6. Lopez-Castejon G, Brough D. Understanding the mechanism of IL-1beta secretion. *Cytokine Growth Factor Rev*. 2011;22:189-195.
7. Fettelschoss A, Kistowska M, LeibundGut-Landmann S, et al. Inflammasome activation and IL-1beta target IL-1alpha for secretion as opposed to surface expression. *Proc Natl Acad Sci USA*. 2011;108:18055-18060.
8. Franchi L, Eigenbrod T, Munoz-Planillo R, Nunez G. The inflammasome: a caspase-1-activation platform that regulates immune responses and disease pathogenesis. *Nat Immunol*. 2009;10:241-247.
9. Abderrazak A, Syrovets T, Couchie D, et al. NLRP3 inflammasome: from a danger signal sensor to a regulatory node of oxidative stress and inflammatory diseases. *Redox Biol*. 2015;4:296-307.
10. Szekanecz Z, Szamosi S, Kovacs GE, Kocsis E, Benko S. The NLRP3 inflammasome - interleukin 1 pathway as a therapeutic target in gout. *Arch Biochem Biophys*. 2019;670:82-93.
11. Crofford LJ. Use of NSAIDs in treating patients with arthritis. *Arthritis Res Ther*. 2013;15(Suppl 3):S2.
12. Schlesinger N. Management of acute and chronic gouty arthritis: present state-of-the-art. *Drugs*. 2004;64:2399-2416.
13. Lionberger DR, Brennan MJ. Topical nonsteroidal anti-inflammatory drugs for the treatment of pain due to soft tissue injury: diclofenac epolamine topical patch. *J Pain Res*. 2010;3:223-233.
14. Fassett RG, Coombes JS. Astaxanthin: a potential therapeutic agent in cardiovascular disease. *Marine drugs*. 2011;9:447-465.
15. Yeh PT, Huang HW, Yang CM, Yang WS, Yang CH. Astaxanthin inhibits expression of retinal oxidative stress and inflammatory mediators in streptozotocin-induced diabetic rats. *PLoS ONE*. 2016;11:e0146438.
16. Okai Y, Higashi-Okai K. Possible immunomodulating activities of carotenoids in in vitro cell culture experiments. *Int J Immunopharmacol*. 1996;18:753-758.
17. Nakao R, Nelson OL, Park JS, Mathison BD, Thompson PA, Chew BP. Effect of astaxanthin supplementation on inflammation and cardiac function in BALB/c mice. *Anticancer Res*. 2010;30:2721-2725.
18. Jyonouchi H, Sun S, Gross M. Effect of carotenoids on in vitro immunoglobulin production by human peripheral blood mononuclear cells: astaxanthin, a carotenoid without vitamin A activity, enhances in vitro immunoglobulin production in response to a T-dependent stimulant and antigen. *Nutr Cancer*. 1995;23:171-183.
19. Chew BP, Wong MW, Park JS, Wong TS. Dietary beta-carotene and astaxanthin but not canthaxanthin stimulate splenocyte function in mice. *Anticancer Res*. 1999;19:5223-5227.
20. Lee HS, Lee CH, Tsai HC, Salter DM. Inhibition of cyclooxygenase 2 expression by diallyl sulfide on joint inflammation induced by urate crystal and IL-1beta. *Osteoarthritis Cartilage*. 2009;17:91-99.
21. Liu FC, Lu JW, Chien CY, et al. Arthroprotective effects of Cf-02 sharing structural similarity with quercetin. *Int J Mol Sci*. 2018;19:1–14.
22. Choi HD, Kang HE, Yang SH, Lee MG, Shin WG. Pharmacokinetics and first-pass metabolism of astaxanthin in rats. *Br J Nutr*. 2011;105:220-227.
23. Jhang JJ, Lin JH, Yen GC. Beneficial properties of phytochemicals on NLRP3 inflammasome-mediated gout and complication. *J Agric Food Chem*. 2018;66:765-772.
24. Grebe A, Hoss F, Latz E. NLRP3 Inflammasome and the IL-1 pathway in atherosclerosis. *Circ Res*. 2018;122:1722-1740.
25. Chen B, Li H, Ou G, Ren L, Yang X, Zeng M. Curcumin attenuates MSU crystal-induced inflammation by inhibiting the degradation

of IkappaBalpha and blocking mitochondrial damage. *Arthritis Res Ther*. 2019;21:193.

26. Choi HK, Mount DB, Reginato AM. Pathogenesis of gout. *Ann Intern Med*. 2005;143:499-516.

27. Pope RM, Tschopp J. The role of interleukin-1 and the inflammasome in gout: implications for therapy. *Arthritis Rheum*. 2007;56:3183-3188.

28. Schroder K, Zhou R, Tschopp J. The NLRP3 inflammasome: a sensor for metabolic danger? *Science*. 2010;327:296-300.

29. Fam AG. Treating acute gouty arthritis with selective COX 2 inhibitors. *BMJ*. 2002;325:980-981.

30. Hochberg MC. COX-2 selective inhibitors in the treatment of arthritis: a rheumatologist perspective. *Curr Top Med Chem*. 2005;5:443-448.

31. Zhang Y, Zheng Y, Li H. NLRP3 inflammasome plays an important role in the pathogenesis of collagen-induced arthritis. *Mediators Inflamm*. 2016;2016:9656270.

32. Liu-Bryan R. Intracellular innate immunity in gouty arthritis: role of NALP3 inflammasome. *Immunol Cell Biol*. 2010;88:20-23.

33. Park JS, Chyun JH, Kim YK, Line LL, Chew BP. Astaxanthin decreased oxidative stress and inflammation and enhanced immune response in humans. *Nutr Metab (Lond)*. 2010;7:18.

34. Miyachi M, Matsuno T, Asano K, Mataga I. Anti-inflammatory effects of astaxanthin in the human gingival keratinocyte line NDUSD-1. *J Clin Biochem Nutr*. 2015;56:171-178.

35. Tripathi DN, Jena GB. Astaxanthin inhibits cytotoxic and genotoxic effects of cyclophosphamide in mice germ cells. *Toxicology*. 2008;248:96-103.

36. Jyonouchi H, Sun S, Iijima K, Gross MD. Antitumor activity of astaxanthin and its mode of action. *Nutr Cancer*. 2000;36:59-65.

37. Coleman JW. Nitric oxide in immunity and inflammation. *Int Immunopharmacol*. 2001;1:1397-1406.

38. Tripathi P, Tripathi P, Kashyap L, Singh V. The role of nitric oxide in inflammatory reactions. *FEMS Immunol Med Microbiol*. 2007;51:443-452.

39. Ricciotti E, FitzGerald GA. Prostaglandins and inflammation. *Arterioscler Thromb Vasc Biol*. 2011;31:986-1000.

40. Giroux M, Descoteaux A. Cyclooxygenase-2 expression in macrophages: modulation by protein kinase C-alpha. *J Immunol*. 2000;165:3985-3991.

SUPPORTING INFORMATION

Additional Supporting Information may be found online in the Supporting Information section.

How to cite this article: Peng Y-J, Lu J-W, Liu F-C, et al. Astaxanthin attenuates joint inflammation induced by monosodium urate crystals. *The FASEB Journal*. 2020;00:1–12. https://doi.org/10.1096/fj.202000558RR